A micro-mechanical constitutive model for heterogeneous rocks with non-associated plastic matrix as implicit standard materials

Lun-Yang Zhao, Jian-Fu Shao, Yuan-Ming Lai, Qi-Zhi Zhu, Jean-Baptiste Colliat, Jian-Fu Shao

A micro-mechanical constitutive model for heterogeneous rocks with non-associated plastic matrix as implicit standard materials

Lun-Yang Zhao[a,b,c], Jian-Fu Shao[b,c,*], Yuan-Ming Lai[a,d], Qi-Zhi Zhu[c], Jean-Baptiste Colliat[b]

[a] *South China Research Institute on Geotechnical Engineering, School of Civil Engineering and Transportation, South China University of Technology, Guangzhou, 510641, China*
[b] *University of Lille, CNRS, Centrale Lille, LaMcube UMR9013, 59000 Lille, France*
[c] *Key Laboratory of Ministry of Education for Geomechanics and Embankment Engineering, Hohai University, Nanjing 210098, China*
[d] *State Key Laboratory Frozen Soil Engineering, Cold and Arid Region Environmental and Engineering Institute, Chinese Academy of Sciences, Lanzhou, Gansu 730000, China*

Abstract

In this work, we shall propose a new micro-mechanical constitutive model for the estimation of effective elastic-plastic behaviors of heterogeneous rocks. A bi-potential based incremental variational (BIV) approach is developed in order to take into account non-uniform local strain fields of constituents. The studied materials are composed of a non-associated and pressure sensitive plastic matrix, elastic inclusions and/or voids. For clarity, the local behavior of matrix is first described by an elastic perfectly-plastic model. Based on the bi-potential theory to dealing with non-associated plastic flow, the solid matrix is considered as pertaining to implicit standard materials (ISMs). The effective incremental bi-potential and macroscopic stress tensor are then estimated through an extension of the incremental variational method initially established for generalized standard materials(GSMs). The accuracy of the BIV model is verified by comparing the model's predictions with the reference results obtained from direct finite element simulations. Furthermore, by assuming that the general formulation obtained for the perfectly plastic matrix remains valid for each loading increment, the BIV model is extended to considering that the solid matrix exhibits an isotropic hardening by using an explicit algorithm. The accuracy of the extended BIV model is also validated by a series of comparisons with the reference solutions obtained by direct finite element simulations for both inclusion-reinforced composites and porous materials. Both local and macroscopic responses are compared. As an example of application, the extended BIV model is finally applied to estimating the mechanical responses of typical claystone and sandstone under different loading paths.

Keywords: Micro-mechanics, Nonlinear homogenization, Non-associated plasticity, Heterogeneous rocks, Claystone, Sandstone

*Corresponding authors: jian-fu.shao@polytech-lille

Preprint submitted to Elsevier *December 19, 2020*

1. Introduction

Rocks are usually regarded as typical composites, which are used in a very wide range of engineering constructions. These materials contain different kinds of heterogeneities at different scales. Pores and inclusions are two main families of heterogeneities. Furthermore, these materials are composed of several mineral phases of different properties. The mineral compositions may significantly vary in space, for instance with geological depth. Laboratory studies have shown that the macroscopic physical and mechanical properties of these materials are affected by heterogeneities and mineral compositions. So far, different kinds of macroscopic models, mainly elastic-plastic and damage models have been developed. Directly fitted from laboratory tests, these models are able to correctly reproduce the main features of mechanical behaviors of those materials. However, they are not able to properly consider the effect of heterogeneities and mineralogical compositions on the macroscopic mechanical responses.

Based on linear homogenization techniques, micro-mechanical models have first been established during the last decades for modeling induced damage in brittle rocks (Zhu et al., 2008, 2016, Zhao et al., 2018, Zhang et al., 2019). Important advances have also been obtained on micro-mechanical modeling of plastic deformation in ductile and porous rocks by using nonlinear homogenization methods. For instance, clayey rocks have been characterized as composites constituted of a plastic clay matrix in which calcite and quartz grains are embedded (Guéry et al., 2008, Jiang et al., 2009). In some multi-scale models, the microstructure of clayey rocks has further been enriched by considering the clay matrix as a porous material at the microscopic scale (Shen et al., 2012). The effective inelastic behavior of the porous clay matrix has been estimated by using the Hill incremental method (Hill, 1965). As for metallic composite materials, it was found that the use of the original Hill's incremental method produced too stiff mechanical behaviors (Suquet, 1996, Chaboche et al., 2005). The main reason is the fact that uniform local strain fields are assumed in constituents of composites in the Hill's method. In order to improve the numerical performance of this method, artificial techniques, such as isotropization of tangent elastic-plastic stiffness tensor, have been proposed. This correction technique has also been applied to clayey rocks (Guéry et al., 2008, Jiang and Shao, 2009, Shen et al., 2012). However, all those correction techniques are generally not based on any physical background.

Meanwhile, advanced nonlinear homogenization techniques have been developed for composite materials considering non-uniform local fields in constituent phases (Castañeda, 1991, 1992, 2002, Lahellec and Suquet, 2007a,b, 2013, Boudet et al., 2016, Brassart et al., 2011, 2012, Danas and Castañeda, 2012), just to mention some representative ones. In particular, variational principles based on the use of a ”linear comparison composite (LCC)” were proposed for the mean field homogenization method of nonlinear elastic composites (Castañeda, 1991, 1992, 2002), and used to generate improved bounds and more generate estimates for the nonlinear elastic-plastic composites (Castañeda and Suquet, 1997, Danas and Castañeda, 2012). By extending these previous works, a new incremental variational method has been established (Lahellec and Suquet, 2007a,b) for modeling effective nonlinear properties of viscoelastic composites without local threshold or hardening. In this new method, equivalent interval variables (EIV) are introduced to capture the non-uniform local plastic strain fields. Further, the same authors have proposed a rate variational model (RVP) by considering a non-uniform field of plastic strain rate (Lahellec and Suquet, 2013). More recently, the EIV method has been extended to modeling elastic-(visco)plastic composites with local threshold and isotropic and/or linear kinematic hardening (Boudet et al., 2016). On the other hand, based on the variational principle established in Ortiz and Stainier (1999), alternative incremental variational models have been proposed in Brassart et al. (2011, 2012) for studying elastic-(visco)plastic composites with local isotropic hardening. The EIV method has further been extended to the description of geological materials with a pressure-dependent Drucker-Prager plastic matrix (Zhao et al., 2019). However, all these previous models have been developed in the scope of Generalized Standard Materials (GSMs) (Halphen and Nguyen, 1975) with an associated plastic flow rule.

Extensive experimental results have clearly shown that for most rocks, a non-associated plastic flow rule is required for correctly modeling the coupling between shear and volumetric strains. These materials cannot be considered as Generalized Standard Materials. As a first approximation, the microstructure of these materials at a selected relevant length scale, for instance micrometer, can be characterized by the representative unit cell shown in Figure 1. Several sets of elastic inclusions (mineral grains in rocks) are embedded in a plastic matrix (clay matrix in clayey rocks). The local behavior of the matrix is generally described by a non-associated and pressure sensitive plastic model. The incremental variational methods developed for the GSMs cannot be directly used to estimate the effective mechanical behaviors of rocks.

In order to generalize the incremental variational principles to heterogeneous rocks, the idea here is first to transform these non-GSMs into a class of implicit standard materials (ISMs). This is done with the help of the bi-potential theory initially developed for macroscopic elastic and plastic behaviors of non-GSMs (De Saxcé and Feng, 1991, De Saxcé and Bousshine, 1998, De Saxcé, 1995). This theory has been successfully used for modeling soils and rock-like materials with non-associated plastic models (Bodovillé and De Saxcé, 2001, Bodovillé, 2001, Hjiaj et al., 2003, Berga, 2012). More-

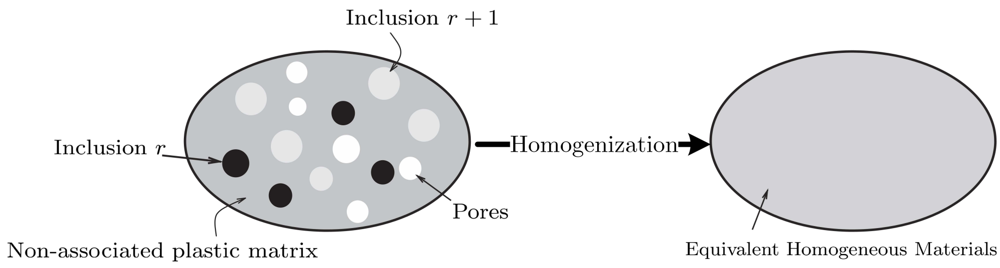

Figure 1: Representative volume element (RVE) of heterogeneous rocks at a selected length scale

over, the bi-potential theory is naturally suitable for developing a variational approach of constitutive modeling.

With the help of the bi-potential theory, the aim of this work is to develop a new incremental variational method for estimating the effective elastic-plastic behavior of heterogeneous rocks composed of a non-associated and pressure sensitive plastic matrix. This is based on the construction of an incremental elastic-plastic bi-potential for ISMs by using an implicit time-discretization scheme.

On the other hand, ductile and porous heterogeneous rocks generally exhibit plastic hardening. For instance, in the case of an isotropic hardening, the internal friction or cohesion can evolve during plastic deformation. In the case of heterogeneous rocks idealized in Figure 1, plastic hardening occurs in the plastic matrix. This mechanism should be taken into account. However, the formulation of an incremental variational model for materials with a pressure-sensitive plastic matrix with plastic hardening may becomes mathematically very complex. By taking the incremental nature of the approach, a simplified explicit method is proposed in this paper. The new bi-potential base incremental variational model (BIV) is first developed by considering a perfectly plastic matrix. Then at the end of each loading increment, the plastic properties are updated but frozen for next loading increment. The plastic matrix is then considered as a material without hardening during the current increment.

The proposed new BIV model is validated by comparing model's predictions and numerical results issued from direct finite element simulations for both perfectly plastic and plastic with hardening cases. Finally, the new BIV model is applied to estimating the effective mechanical responses of typical claystone and porous sandstone in various loading paths.

Throughout this paper, the following notions of tensorial products of any second order tensors $\boldsymbol{A}$ and $\boldsymbol{B}$ will be used: $(\boldsymbol{A} \otimes \boldsymbol{B})_{ijkl} = A_{ij}B_{kl}$ and $\boldsymbol{A} : \boldsymbol{B} = A_{ij}B_{ij}$. Fourth order tensors are denoted by blackboard bold characters, and one can define $(\mathbb{C} : \boldsymbol{B})_{kl} = C_{ijkl}B_{kl}$. The symbol $\|\boldsymbol{A}\| = \sqrt{\boldsymbol{A} : \boldsymbol{A}}$ is used to denote the norm of any second order tensor $\boldsymbol{A}$. With the second order identity tensor $\boldsymbol{\delta}$, usually used fourth order isotropic identity tensor $\mathbb{I}$ and fourth order hydrostatic projects $\mathbb{J}$ are expressed in the components form as $I_{ijkl} = \frac{1}{2}\left(\delta_{ik}\delta_{jl} + \delta_{il}\delta_{jk}\right)$ and $J_{ijkl} = \frac{1}{3}\delta_{ij}\delta_{kl}$, respectively. The fourth order deviatoric projects $\mathbb{K} = \mathbb{I} - \mathbb{J}$ is then obtained. Moreover, the fourth-order tensors $\mathbb{J}$ and $\mathbb{K}$ have the properties: $\mathbb{J} : \mathbb{J} = \mathbb{J}$, $\mathbb{K} : \mathbb{K} = \mathbb{K}$, $\mathbb{J} : \mathbb{K} = \mathbb{K} : \mathbb{J} = \mathbf{0}$.

2. Bi-potential theory for non-associated plastic flow rule

2.1. Generalized standard materials (GSM)

A large class of solid materials can be described by using a generalized framework based on the existence of two convex potentials conjugating one to the other $V(\dot{\boldsymbol{\varepsilon}})$ and $W(\boldsymbol{\sigma})$ satisfying the Fenchel's inequality (Fenchel, 1949)

$$\forall\, (\boldsymbol{\sigma}, \dot{\boldsymbol{\varepsilon}}) \quad W(\boldsymbol{\sigma}) + V(\dot{\boldsymbol{\varepsilon}}) \geq \boldsymbol{\sigma} : \dot{\boldsymbol{\varepsilon}} \tag{1}$$

where $\boldsymbol{\sigma}$ is the Cauchy stress tensor and $\dot{\boldsymbol{\varepsilon}}$ is the strain rate tensor. A pair of $(\boldsymbol{\sigma}, \dot{\boldsymbol{\varepsilon}})$ is said to be extremal if the equality is achieved, that is:

$$W(\boldsymbol{\sigma}) + V(\dot{\boldsymbol{\varepsilon}}) = \boldsymbol{\sigma} : \dot{\boldsymbol{\varepsilon}} \tag{2}$$

Then, any extremal pair is characterized by the following relations:

$$\forall \boldsymbol{\sigma}' \quad W(\boldsymbol{\sigma}') - W(\boldsymbol{\sigma}) \;\; \geq \;\; (\boldsymbol{\sigma}' - \boldsymbol{\sigma}) : \dot{\boldsymbol{\varepsilon}} \tag{3a}$$

$$\forall \dot{\boldsymbol{\varepsilon}}' \quad V(\dot{\boldsymbol{\varepsilon}}') - V(\dot{\boldsymbol{\varepsilon}}) \;\; \geq \;\; \boldsymbol{\sigma} : (\dot{\boldsymbol{\varepsilon}}' - \dot{\boldsymbol{\varepsilon}}) \tag{3b}$$

Therefore, $\boldsymbol{\sigma}$ and $\dot{\boldsymbol{\varepsilon}}$ are expressed by the sub-differential mappings

$$\boldsymbol{\sigma} = \frac{\partial V}{\partial \dot{\boldsymbol{\varepsilon}}}(\dot{\boldsymbol{\varepsilon}}), \quad \dot{\boldsymbol{\varepsilon}} = \frac{\partial W}{\partial \boldsymbol{\sigma}}(\boldsymbol{\sigma}) \tag{4}$$

These relations constitute the normality rule. Different kinds of constitutive equations, such as plastic laws, visco-plastic law and plastic hardening laws can generally and conveniently be constructed with Eq.(4). The class of materials governed by the two convex potentials are called generalized standard materials (GSMs) (Halphen and Nguyen, 1975).

2.2. Implicit standard material

However, the mechanical behavior of a large number of materials cannot be integrated within the above framework. For example, for most heterogeneous rocks, one of the constituent phase exhibits a plastic or viscoplastic behavior which is generally described by a non-associated flow rule. The normality rule is then not verified. Conventional approaches for modeling the non-associated plastic deformation are based on the choice of two independent functions of stress tensor, the plastic yield function to determine yield locus and the plastic potential function giving the plastic strain evolution law. However, this type of approaches loses the good property of convexity (De Saxcé, 1995, Berga, 2012). The bi-potential theory proposed by De Saxcé and Feng (1991) provides a convenient mathematical frame for dealing with non-associated plastic materials. It allows keeping the key-concept of normality and convexity. This theory generalizes the Fenchel's inequality to materials and systems with non-standard behaviour. To find the concept of normal dissipation, the constitutive laws are formulated under an implicit form. For the sake of clarity, the basic notion of implicit standard materials (ISMs) is here recalled (De Saxcé and Feng, 1991).

For describing the behaviour of ISMs, a bi-potential $b(\boldsymbol{\sigma}, \dot{\boldsymbol{\varepsilon}})$ is first introduced. It is a scalar-valued function, convex with respect to $\boldsymbol{\sigma}$ when $\dot{\boldsymbol{\varepsilon}}$ keeps constant, and convex with respect to $\dot{\boldsymbol{\varepsilon}}$ when $\boldsymbol{\sigma}$ remains constant. The bi-potential function should also verify the following inequality

$$\forall\,(\boldsymbol{\sigma}, \dot{\boldsymbol{\varepsilon}}) \quad b(\boldsymbol{\sigma}, \dot{\boldsymbol{\varepsilon}}) \geq \boldsymbol{\sigma} : \dot{\boldsymbol{\varepsilon}} \tag{5}$$

If and only if the pair $(\boldsymbol{\sigma}, \dot{\boldsymbol{\varepsilon}})$ is obtained at the extreme value, implying that $(\boldsymbol{\sigma}, \dot{\boldsymbol{\varepsilon}})$ satisfies the constitutive relation of the material, one has

$$b(\boldsymbol{\sigma}, \dot{\boldsymbol{\varepsilon}}) = \boldsymbol{\sigma} : \dot{\boldsymbol{\varepsilon}} \tag{6}$$

Then, any extremal pair is characterized by the following relations:

$$\forall \boldsymbol{\sigma}' \quad b(\boldsymbol{\sigma}', \dot{\boldsymbol{\varepsilon}}) - b(\boldsymbol{\sigma}, \dot{\boldsymbol{\varepsilon}}) \;\geq\; (\boldsymbol{\sigma}' - \boldsymbol{\sigma}) : \dot{\boldsymbol{\varepsilon}} \tag{7a}$$

$$\forall \dot{\boldsymbol{\varepsilon}}' \quad b(\boldsymbol{\sigma}, \dot{\boldsymbol{\varepsilon}}') - b(\boldsymbol{\sigma}, \dot{\boldsymbol{\varepsilon}}) \;\geq\; \boldsymbol{\sigma} : (\dot{\boldsymbol{\varepsilon}}' - \dot{\boldsymbol{\varepsilon}}) \tag{7b}$$

Accordingly, $\boldsymbol{\sigma}$ and $\dot{\boldsymbol{\varepsilon}}$ are related by the subnormality laws

$$\boldsymbol{\sigma} = \frac{\partial b}{\partial \dot{\boldsymbol{\varepsilon}}}(\boldsymbol{\sigma}, \dot{\boldsymbol{\varepsilon}}), \quad \dot{\boldsymbol{\varepsilon}} = \frac{\partial_{\sigma} b}{\partial \boldsymbol{\sigma}}(\boldsymbol{\sigma}, \dot{\boldsymbol{\varepsilon}}) \tag{8}$$

These relations provide a multi-valued constitutive relationship between $\boldsymbol{\sigma}$ and $\dot{\boldsymbol{\varepsilon}}$, which is now implicit in the sense of the implicit function theorem. It is noted that GSMs can be considered as particular cases of ISMs with separable bi-potentials:

$$b(\boldsymbol{\sigma}, \dot{\boldsymbol{\varepsilon}}) = W(\boldsymbol{\sigma}) + V(\dot{\boldsymbol{\varepsilon}}) \tag{9}$$

2.3. Incremental elastic-plastic bi-potential

We consider now the local elastic-plastic behavior of the solid matrix in heterogeneous rocks. For the sake of clarity, the behavior of matrix is described by an elastic perfectly plastic non-associated model. Under the assumption of isothermal conditions and small strains, the total strain tensor $\boldsymbol{\varepsilon}$ is decomposed into an elastic part $\boldsymbol{\varepsilon}^e$ and a plastic one $\boldsymbol{\varepsilon}^p$

$$\boldsymbol{\varepsilon} = \boldsymbol{\varepsilon}^e + \boldsymbol{\varepsilon}^p \tag{10}$$

In view of applying the incremental variational method to determining the effective mechanical behavior of heterogeneous rocks, it is needed to derive an incremental elastic-plastic bi-potential for the plastic matrix. To this end, the general forms of the elastic and plastic bi-potentials are first separately formulated. Then the incremental elastic-plastic bi-potential is established by using a time-discretization scheme.

2.3.1. Elastic bi-potential

In the elastic regime, the bi-potential conforms to the characteristics of GSMs. Moreover, the elastic laws can be derived from the strain energy density function $V(\boldsymbol{\varepsilon} - \boldsymbol{\varepsilon}^p)$ and the complementary energy density function $W(\boldsymbol{\sigma})$. Therefore, the elastic bi-potential b_e is a separate function with the following expression

$$b_e(\boldsymbol{\varepsilon},\ \boldsymbol{\varepsilon}^p,\ \boldsymbol{\sigma}) = V(\boldsymbol{\varepsilon} - \boldsymbol{\varepsilon}^p) + W(\boldsymbol{\sigma}) \tag{11}$$

which satisfies the implicit standard laws

$$\boldsymbol{\sigma} = \frac{\partial b_e}{\partial \boldsymbol{\varepsilon}}(\boldsymbol{\varepsilon},\ \boldsymbol{\varepsilon}^p,\ \boldsymbol{\sigma}) = -\frac{\partial b_e}{\partial \boldsymbol{\varepsilon}^p}(\boldsymbol{\varepsilon},\ \boldsymbol{\varepsilon}^p,\ \boldsymbol{\sigma}) \text{ and } \boldsymbol{\varepsilon} = \frac{\partial b_e}{\partial \boldsymbol{\sigma}}(\boldsymbol{\varepsilon},\ \boldsymbol{\varepsilon}^p,\ \boldsymbol{\sigma}) + \boldsymbol{\varepsilon}^p \tag{12}$$

2.3.2. Plastic bi-potential

Under the plastic state, the non-associated plastic model falls into the category of ISMs. By virtue of (5) the plastic bi-potential function is first defined by the condition:

$$\forall\, (\boldsymbol{\sigma}, \dot{\boldsymbol{\varepsilon}}^p) \quad b_p(\boldsymbol{\sigma}, \dot{\boldsymbol{\varepsilon}}^p) \geq \boldsymbol{\sigma} : \dot{\boldsymbol{\varepsilon}}^p \tag{13}$$

Similarly, if and only if the pair $(\boldsymbol{\sigma}, \dot{\boldsymbol{\varepsilon}}^p)$ reaches the extreme value, one gets:

$$b_p(\boldsymbol{\sigma}, \dot{\boldsymbol{\varepsilon}}^p) = \boldsymbol{\sigma} : \dot{\boldsymbol{\varepsilon}}^p \tag{14}$$

Then $\boldsymbol{\sigma}$ and $\dot{\boldsymbol{\varepsilon}}^p$ are related by subnormality laws:

$$\boldsymbol{\sigma} = \frac{\partial b_p}{\partial \dot{\boldsymbol{\varepsilon}}^p}(\boldsymbol{\sigma}, \dot{\boldsymbol{\varepsilon}}^p), \quad \dot{\boldsymbol{\varepsilon}}^p = \frac{\partial b_p}{\partial \boldsymbol{\sigma}}(\boldsymbol{\sigma}, \dot{\boldsymbol{\varepsilon}}^p) \tag{15}$$

2.3.3. *Incremental elastic-plastic bi-potential*

Combining Eqs. (12) and (15), the constitutive relations of the plastic phase under consideration can be expressed as a system of two coupled equations, one of them being a differential equation in time:

$$\boldsymbol{\sigma} = \frac{\partial b_e}{\partial \boldsymbol{\varepsilon}} \left(\boldsymbol{\varepsilon}, \boldsymbol{\varepsilon}^p, \boldsymbol{\sigma}\right) \tag{16a}$$

$$\frac{\partial b_e}{\partial \boldsymbol{\varepsilon}^p} \left(\boldsymbol{\varepsilon}, \boldsymbol{\varepsilon}^p, \boldsymbol{\sigma}\right) + \frac{\partial b_p}{\partial \dot{\boldsymbol{\varepsilon}}^p} \left(\boldsymbol{\sigma},\ \dot{\boldsymbol{\varepsilon}}^p\right) = 0 \tag{16b}$$

Based on the previous work by Ortiz and Stainier (1999), the time derivative $\dot{\boldsymbol{\varepsilon}}^p$ is approximated by a difference quotient after the use of an implicit Eular-Scheme. The whole time period (whole loading history) of study $[0, T]$ is accordingly divided into the time steps (loading steps) $t_0 = 0, t_1, ..., t_n, t_{n+1}, ..., t_N = T$. The time increment between t_n and t_{n+1} (loading increment) is denoted by Δt. For the sake of simplifying the notations, its dependence on n is omitted. By using this time-discretization scheme, the system of differential equations (16) is transformed to the following discretized system:

$$\boldsymbol{\sigma}_{n+1} = \frac{\partial b_e}{\partial\, \boldsymbol{\varepsilon}} \left(\boldsymbol{\varepsilon}_{n+1}, \boldsymbol{\varepsilon}^p_{n+1}, \boldsymbol{\sigma}_{n+1}\right), \quad \frac{\partial b_e}{\partial \boldsymbol{\varepsilon}^p} \left(\boldsymbol{\varepsilon}_{n+1}, \boldsymbol{\varepsilon}^p_{n+1}, \boldsymbol{\sigma}_{n+1}\right) + \frac{\partial b_p}{\partial \dot{\boldsymbol{\varepsilon}}^p} \left(\boldsymbol{\sigma}_{n+1}, \frac{\boldsymbol{\varepsilon}^p_{n+1} - \boldsymbol{\varepsilon}^p_n}{\Delta t}\right) = 0 \tag{17}$$

The values of local fields at time t_{n+1} $(\boldsymbol{\varepsilon}_{n+1}, \boldsymbol{\varepsilon}^p_{n+1}, \boldsymbol{\sigma}_{n+1})$ are unknown, while their values at time t_n $(\boldsymbol{\varepsilon}_n, \boldsymbol{\varepsilon}^p_n, \boldsymbol{\sigma}_n)$ are assumed to be all known. We introduce here the following incremental bi-potential J, a scalar-valued function of variables $\boldsymbol{\varepsilon}$, $\boldsymbol{\varepsilon}^p$and $\boldsymbol{\sigma}$:

$$J\left(\boldsymbol{\varepsilon}, \boldsymbol{\varepsilon}^p, \boldsymbol{\sigma}\right) = b_e(\boldsymbol{\varepsilon}, \boldsymbol{\varepsilon}^p, \boldsymbol{\sigma}) + \Delta t b_p \left(\boldsymbol{\sigma}, \frac{\boldsymbol{\varepsilon}^p - \boldsymbol{\varepsilon}^p_n}{\Delta t}\right) \tag{18}$$

Again, for the sake of abbreviation, the subscripts $n + 1$ are omitted. Notice that the second relation in (17) is the Euler-Lagrange equation of the variational problem for the minimization of incremental bi-potential with respect to $\boldsymbol{\varepsilon}^p$. This leads to the following condensed incremental bi-potential:

$$\pi_\Delta\left(\boldsymbol{\varepsilon}, \boldsymbol{\sigma}\right) = \inf_{\boldsymbol{\varepsilon}^p} J\left(\boldsymbol{\varepsilon}, \boldsymbol{\sigma}, \boldsymbol{\varepsilon}^p\right) \tag{19}$$

After that, the local stress field $\boldsymbol{\sigma}$ can be derived from this sole bi-potential

$$\boldsymbol{\sigma} = \frac{\partial \pi_\Delta}{\partial\, \boldsymbol{\varepsilon}} \left(\boldsymbol{\varepsilon}, \boldsymbol{\sigma}\right) \tag{20}$$

3. Bi-potential based incremental variational method for homogenization of heterogeneous rocks

In this section, a bi-potential theory based incremental variational method (BIV) is developed for the estimation of effective elastic-plastic behavior of heterogenous rocks in the framework of implicit standard materials (ISMs) and with the help of the bi-potential theory defined above.

3.1. Representative Volume Element (RVE) and constituents properties

As already shown in Figure 1, the Representative Volume Element (RVE) of rocks at the selected length scale (micrometer) is composed of an isotropic elastic-plastic solid matrix in which elastic inclusions (mineral grains) or pores are randomly embedded. The RVE occupies the domain $\Omega \subset \mathbb{R}^{n_{\dim}}$ ($n_{\dim} = 1, 2, 3$) with the external boundary $\Omega \subset \mathbb{R}^{n_{\dim}-1}$. The solid matrix occupies the sub-domain $\Omega^m \subset \mathbb{R}^{n_{\dim}}$. The elastic property of the matrix is characterized by the elastic stiffness tensor $\mathbb{C}^m$ and the plastic behavior is described by a non-associated plastic model with Drucker-Prager yield criterion. The r^{th} phase of inclusions occupies the sub-domain $\Omega^{i,r} \subset \mathbb{R}^{n_{\dim}}$, $r = 1, ..., N$, and is characterized by the elastic stiffness tensor $\mathbb{C}^{i,r}$. The phase of pores is here treated as a special inclusion phase with a vanished elastic stiffness.

For the convenience of the subsequent formulation, the total volume of the RVE is denoted as V_Ω, the volume of matrix as V_{Ω^m}, and the volume occupied by the r^{th} inclusion phase as $V_{\Omega^{i,r}}$. Accordingly, the volume fractions of the constituents are given by:

$$f^m = \frac{V_{\Omega^m}}{V_\Omega}; \quad f^{i,r} = \frac{V_{\Omega^{i,r}}}{V_\Omega}, \quad r = 1, ..., N; \tag{21}$$

Further, the operator $\langle \cdot \rangle$ denotes a volume average over the whole RVE, $\langle \cdot \rangle_m$ is a volume average over the matrix, and $\langle \cdot \rangle_{i,r}$ is a volume average over the r^{th} inclusion phase. That is

$$\langle \cdot \rangle = \frac{1}{V_\Omega} \int_{V_\Omega} (\cdot) \, \mathrm{d}V_\Omega = f^m \langle \cdot \rangle_m + \sum_{r=1}^{N} f^{i,r} \langle \cdot \rangle_{i,r} \tag{22}$$

with

$$\langle \cdot \rangle_m = \frac{1}{V_{\Omega^m}} \int_{V_{\Omega^m}} (\cdot) \, \mathrm{d}V_{\Omega^m}; \quad \langle \cdot \rangle_{i,r} = \frac{1}{V_{\Omega^{i,r}}} \int_{V_{\Omega^{i,r}}} (\cdot) \, \mathrm{d}V_{\Omega^{i,r}} \tag{23}$$

3.1.1. Incremental bi-potential of the elastic and non-associated Drucker-Prager perfectly plastic matrix

By assuming that the elastic behaviour is independent of irreversible process, the elastic bi-potential $b_e^m(\boldsymbol{\varepsilon}, \boldsymbol{\varepsilon}^p, \boldsymbol{\sigma})$ at any point $\underline{x} \in \Omega^m$ is written as:

$$b_e^m(\boldsymbol{\varepsilon}, \boldsymbol{\varepsilon}^p, \boldsymbol{\sigma}) = \frac{1}{2} (\boldsymbol{\varepsilon} - \boldsymbol{\varepsilon}^p) : \mathbb{C}^m : (\boldsymbol{\varepsilon} - \boldsymbol{\varepsilon}^p) + \frac{1}{2} \boldsymbol{\sigma} : \mathbb{S}^m : \boldsymbol{\sigma} \tag{24}$$

where the isotropic elastic stiffness tensor is expressed as $\mathbb{C}^m = 3k^m \mathbb{J} + 2\mu^m \mathbb{K}$, with k^m and μ^m being the bulk modulus and shear modulus of the matrix respectively. $\mathbb{S}^m = [\mathbb{C}^m]^{-1}$ is the elastic compliance tensor.

The Drucker-Prager plastic yield function is illustrated in Figure 2 and is written as:

$$\mathcal{F}(\boldsymbol{\sigma}) = \sigma_{eq} + 3\kappa (\sigma_m - c) \leq 0 \tag{25}$$

where $\sigma_{eq} = \sqrt{\frac{3}{2}\boldsymbol{s} : \boldsymbol{s}}$ is the equivalent stress (with $\boldsymbol{s} = \boldsymbol{\sigma} : \mathbb{K}$), and $\sigma_m = \frac{1}{3}\boldsymbol{\sigma} : \boldsymbol{\delta}$ the mean stress. The parameter c and κ respectively represent the hydrostatic tensile strength and friction coefficient. It is noted that κ is related to the friction angle ϕ as follows:

$$\tan\phi = 3\kappa \tag{26}$$

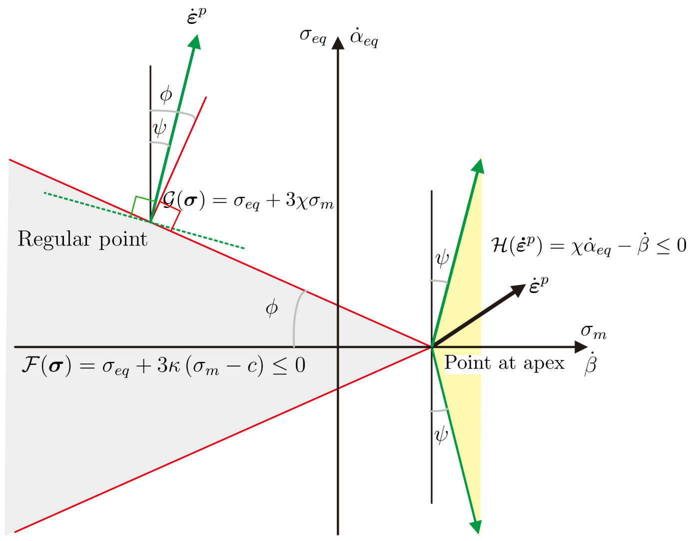

Figure 2: Drucker-Prager yield surface and non-associated plastic flow rule

The non-associated plastic flow rule is defined by the following plastic potential:

$$\mathcal{G}(\boldsymbol{\sigma}) = \sigma_{eq} + 3\chi\sigma_m \tag{27}$$

where χ denotes the plastic dilatancy coefficient, which depends on the dilatancy angle ψ:

$$\tan\psi = 3\chi \tag{28}$$

Further, for any stress state located on the regular part of the yield surface, it is assumed that the plastic dilatancy coefficient χ is equal or less than the friction coefficient, i.e., $\chi \leq \kappa$ (Hjiaj et al., 2003). The corresponding rate form of plastic strain $\boldsymbol{\varepsilon}^p$ is defined by the non-associated flow rule:

$$\dot{\boldsymbol{\varepsilon}}^p = \dot{\gamma}^p \frac{\partial \mathcal{G}}{\partial \boldsymbol{\sigma}} = \dot{\gamma}^p \left(\frac{3}{2} \frac{\boldsymbol{s}}{\sigma_{eq}} + \chi \boldsymbol{\delta} \right) \tag{29}$$

where γ^p is a non-negative internal variable acting as the plastic multiplier. For convenience, the plastic strain tensor is decomposed into a spherical part and a deviatoric part:

$$\boldsymbol{\varepsilon}^p = \boldsymbol{\alpha} + \boldsymbol{\beta},\ \boldsymbol{\alpha} = \boldsymbol{\varepsilon}^p : \mathbb{K},\ \ \boldsymbol{\beta} = \boldsymbol{\varepsilon}^p : \mathbb{J} = \frac{1}{3}\mathrm{tr}\boldsymbol{\varepsilon}^p\boldsymbol{\delta} = \beta\boldsymbol{\delta} \tag{30}$$

One thus obtains:

$$\dot{\gamma}^p = \sqrt{\frac{2}{3}\dot{\boldsymbol{\alpha}} : \dot{\boldsymbol{\alpha}}} = \dot{\alpha}_{eq}, \quad \dot{\boldsymbol{\alpha}} = \mathbb{K} : \dot{\boldsymbol{\varepsilon}}^p, \quad \dot{\beta} = \frac{1}{3}\mathrm{tr}\dot{\boldsymbol{\varepsilon}}^p = \chi\dot{\alpha}_{eq} \tag{31}$$

Again for convenience we introduce

$$\mathcal{H}(\dot{\boldsymbol{\varepsilon}}^p) = \chi\dot{\alpha}_{eq} - \dot{\beta} \tag{32}$$

Considering now a stress state at the apex point ($\sigma_{eq} = 0, \sigma_m = c$) of the Drucker-Prager yield surface, $\mathcal{F}(\boldsymbol{\sigma})$ is not differentiable, and the plastic strain rate tensor is not unique. In this case, one gets $\mathcal{H}(\dot{\boldsymbol{\varepsilon}}^p) \leq 0$ (see Figure 2). It is obviously noticed from Eq. (31) that $\mathcal{H}(\dot{\boldsymbol{\varepsilon}}^p) = 0$ for the points on the regular part of the yield surface. Therefore, the plastic flow rule (29) is completed by the admissibility condition of the plastic strain rate for all the cases

$$\mathcal{H}(\dot{\boldsymbol{\varepsilon}}^p) \leq 0 \tag{33}$$

According to Hjiaj et al. (2003), the plastic bi-potential for the non-associated Drucker-Prager plastic flow without strain hardening takes the following form:

$$b_p^m(\boldsymbol{\sigma}, \dot{\boldsymbol{\varepsilon}}^p) = \begin{cases} 3c\dot{\beta} + 3(\chi - \kappa)(\sigma_m - c)\dot{\alpha}_{eq} & \text{if } \mathcal{F}(\boldsymbol{\sigma}) \leq 0 \text{ and } \mathcal{H}(\dot{\boldsymbol{\varepsilon}}^p) \leq 0 \\ +\infty & \text{otherwise} \end{cases} \tag{34}$$

The proof that the function (34) is a bi-potential has been given in Hjiaj et al. (2003).It is noted that the above express is defined for the regular stress points. In this case, the function (34) can be further rewritten as

$$b_p^m(\boldsymbol{\sigma}, \dot{\boldsymbol{\varepsilon}}^p) = b_p^m(\boldsymbol{\sigma}, \dot{\boldsymbol{\alpha}}) = \begin{cases} \underbrace{[3\sigma_m(\chi - \kappa) + 3c\kappa]}_{\sigma_y}\dot{\alpha}_{eq} = \sigma_y\dot{\alpha}_{eq} & \text{if } \mathcal{F}(\boldsymbol{\sigma}) \leq 0 \text{ and } \mathcal{H}(\dot{\boldsymbol{\varepsilon}}^p) = 0 \\ +\infty & \text{otherwise} \end{cases} \tag{35}$$

Remark 1. The second part of the first line in the right hand side of Eq. (35) contains a mixed term of stress and plastic strain rate. When $\chi = \kappa$, the mixed term disappears and the bi-potential $b_p^m(\boldsymbol{\sigma}, \dot{\boldsymbol{\alpha}})$ reduces to the plastic dissipation potential $\varphi^m(\dot{\boldsymbol{\alpha}})$ for GSMs.

$$b_p^m(\boldsymbol{\sigma}, \dot{\boldsymbol{\alpha}}) = \varphi^m(\dot{\boldsymbol{\alpha}}) = \begin{cases} 3c\kappa\dot{\alpha}_{eq} & \text{if } f(\boldsymbol{\sigma}) \leq 0 \text{ and } \mathcal{H}(\dot{\boldsymbol{\varepsilon}}^p) = 0 \\ +\infty & \text{otherwise} \end{cases} \tag{36}$$

Inserting the elastic bi-potential (24) and plastic bi-potential(35) into Eq.(19), one finally obtains the local incremental bi-potential π_Δ^m of the elastic non-associated perfectly plastic matrix:

$$\pi_\Delta^m(\boldsymbol{\varepsilon}, \boldsymbol{\sigma}) = \inf_{\boldsymbol{\varepsilon}^p} J^m(\boldsymbol{\varepsilon}, \boldsymbol{\sigma}, \boldsymbol{\varepsilon}^p) = \inf_{\boldsymbol{\varepsilon}^p}\left(b_e^m(\boldsymbol{\varepsilon}, \boldsymbol{\varepsilon}^p, \boldsymbol{\sigma}) + \Delta t b_p^m\left(\boldsymbol{\sigma}, \frac{\boldsymbol{\varepsilon}^p - \boldsymbol{\varepsilon}_n^p}{\Delta t}\right)\right) \tag{37}$$

3.1.2. Behavior of elastic inclusion

At any point inside the r^{th} linear elastic inclusion phase, i.e., $\underline{x} \in \Omega^{i,r}$, the elastic bi-potential $b_e^{i,r}$ is the convex function of local strain field $\boldsymbol{\varepsilon}$ and stress field $\boldsymbol{\sigma}$. Accordingly, the local incremental bi-potential $\pi_\Delta^{i,r}$ of the r^{th} elastic inclusion phase is expressed as:

$$\pi_\Delta^{i,r} = b_e^{i,r}(\boldsymbol{\varepsilon}, \boldsymbol{\sigma}) = \frac{1}{2}\boldsymbol{\varepsilon} : \mathbb{C}^{i,r} : \boldsymbol{\varepsilon} + \frac{1}{2}\boldsymbol{\sigma} : \mathbb{S}^{i,r} : \boldsymbol{\sigma} \tag{38}$$

3.2. Effective behavior of heterogeneous rocks

We consider that the RVE of heterogeneous rocks is subjected to a macroscopic strain $\overline{\boldsymbol{\varepsilon}}(t)$, and for definiteness, to the periodic kinematic boundary conditions on its boundary $\partial\Omega$ at time step t_{n+1}. Due to the time-discretization scheme adopted, the local problem to be solved is formulated as follows:

$$\left\{\begin{array}{l} \operatorname{div} \boldsymbol{\sigma}_{n+1} = 0 \\ \boldsymbol{\sigma}_{n+1} = \frac{\partial \pi_\Delta}{\partial \boldsymbol{\varepsilon}_{n+1}}(\boldsymbol{\varepsilon}_{n+1}, \boldsymbol{\sigma}_{n+1}) \\ \langle \boldsymbol{\varepsilon}(t) \rangle = \overline{\boldsymbol{\varepsilon}}(t) + BC \;\; \text{on } \partial\Omega \end{array}\right\} \quad \text{for } \left(\underline{x}, t\right) \in \Omega \times [0, T] \tag{39}$$

The condensed incremental bi-potential $\pi_\Delta\left(\underline{x}, \boldsymbol{\varepsilon}, \boldsymbol{\sigma}\right)$ in the RVE is here defined as:

$$\pi_\Delta = \begin{cases} \pi_\Delta^m & \text{if } \underline{x} \in \Omega^m \\ \pi_\Delta^{i,r} & \text{if } \underline{x} \in \Omega^{i,r} \end{cases} \tag{40}$$

Finally, the macroscopic stress $\bar{\boldsymbol{\sigma}}$ can be derived from the effective incremental bi-potential of the RVE:

$$\bar{\boldsymbol{\sigma}}_{n+1} = \frac{\partial \Pi_\Delta}{\partial \bar{\boldsymbol{\varepsilon}}}(\bar{\boldsymbol{\varepsilon}}_{n+1}, \bar{\boldsymbol{\sigma}}_{n+1}) \tag{41}$$

The effective incremental bi-potential Π_Δ is here determined by using the variational principle:

$$\Pi_\Delta(\bar{\boldsymbol{\varepsilon}}_{n+1}, \bar{\boldsymbol{\sigma}}_{n+1}) = \inf_{\langle \boldsymbol{\varepsilon} \rangle = \bar{\boldsymbol{\varepsilon}}_{n+1}} \langle \pi_\Delta \rangle = \inf_{\langle \boldsymbol{\varepsilon} \rangle = \bar{\boldsymbol{\varepsilon}}_{n+1}} \left[f^m \left\langle \inf_{\boldsymbol{\varepsilon}^p} J^m(\boldsymbol{\varepsilon}, \boldsymbol{\varepsilon}^p, \boldsymbol{\sigma}) \right\rangle_m + \sum_{r=1}^{N} f^{i,r} \left\langle b_e^{i,r}(\boldsymbol{\varepsilon}, \boldsymbol{\sigma}) \right\rangle_{i,r} \right] \tag{42}$$

The effective incremental bi-potential of the RVE is not only related to the macroscopic strain $\bar{\boldsymbol{\varepsilon}}$, but also to the average value of local stress filed $\boldsymbol{\sigma}$ on the RVE. With this single effective bi-potential in hand, according to Eq. (41), the macroscopic stress is the conjugated force associated with the macroscopic strain, which is consistent with the classical thermodynamic framework. Moreover, the macroscopic stress defined here also coincides with the volumetric average of the local stress field over the RVE. Accordingly, the problem of computing the overall response of the heterogeneous materials comes to solving the variational problem (42) at each time step, which itself involves a local optimization problem (37) with respect to the internal variables (plastic strain) $\boldsymbol{\varepsilon}^p$ at every position $\underline{x} \in \Omega^m$. Instead of searching a computationally-costly full-field numerical solution, an approximated solutions is found in Section 4 by using the variational procedure initially proposed in Lahellec and Suquet (2007b) for GSMs.

4. Optimization of the effective incremental bi-potential

The main steps for the estimation of the effective incremental bi-potential through a variational procedure are presented in this section.

4.1. Approximation of local incremental bi-potential of the elastic perfectly-plastic matrix

The first step is to approximate the local incremental bi-potential J^m given in (37). It is noticed that the elastic bi-potential given in (24) includes the plastic volumetric strain $\boldsymbol{\beta}$. For ease of calculation and taking advantage of the main results obtained in Lahellec and Suquet (2007b), the elastic bi-potential (24) is approximated and the plastic bi-potential (35) is linearized as follows.

- Approximation of local elastic bi-potential $b_e(\boldsymbol{\varepsilon}, \boldsymbol{\varepsilon}^p, \boldsymbol{\sigma})$ (see detailed process in Appendix A)

$$b_e^m(\boldsymbol{\varepsilon}, \boldsymbol{\varepsilon}^p, \boldsymbol{\sigma}) \simeq b_e^{app}(\boldsymbol{\varepsilon}, \boldsymbol{\alpha}) = \frac{1}{2}\boldsymbol{\sigma} : \mathbb{S}^m : \boldsymbol{\sigma} + \frac{1}{2}\left(\boldsymbol{\varepsilon} - \boldsymbol{\alpha} - \langle \boldsymbol{\beta}_n \rangle_m - \overline{\overline{\boldsymbol{\alpha} - \boldsymbol{\alpha}_n}}\chi\boldsymbol{\delta}\right) : \mathbb{C}^m : \left(\boldsymbol{\varepsilon} - \boldsymbol{\alpha} - \langle \boldsymbol{\beta}_n \rangle_m - \overline{\overline{\boldsymbol{\alpha} - \boldsymbol{\alpha}_n}}\chi\boldsymbol{\delta}\right) \tag{43}$$

- For the plastic bi-potential $b^p(\boldsymbol{\sigma}, \dot{\boldsymbol{\alpha}})$ here we use the same variational linearization procedure and take the same quadratic form as those used in Lahellec and Suquet (2007b) and Boudet et al. (2016), i.e. $\frac{\eta_0}{\Delta t}(\boldsymbol{\alpha} - \tilde{\boldsymbol{\alpha}}_n) : (\boldsymbol{\alpha} - \tilde{\boldsymbol{\alpha}}_n)$. In this expression, the scalar variable η_0 and second-order tensor $\tilde{\boldsymbol{\alpha}}_n$ are uniform in the elastic-plastic matrix.

With the above simplifications in hand, the local incremental bi-potential J^m in (37) can be approximated as

$$\begin{cases} J^m(\boldsymbol{\varepsilon}, \boldsymbol{\varepsilon}^p, \boldsymbol{\sigma}) \simeq J_0^m(\boldsymbol{\varepsilon}, \boldsymbol{\alpha}) + \Delta J^m(\boldsymbol{\sigma}, \boldsymbol{\alpha}) \\ J_0^m(\boldsymbol{\varepsilon}, \boldsymbol{\alpha}) = \frac{1}{2}\left(\boldsymbol{\varepsilon} - \boldsymbol{\alpha} - \langle \boldsymbol{\beta}_n \rangle_m - \overline{\overline{\boldsymbol{\alpha} - \boldsymbol{\alpha}_n}}\chi\boldsymbol{\delta}\right) : \mathbb{C}^m : \left(\boldsymbol{\varepsilon} - \boldsymbol{\alpha} - \langle \boldsymbol{\beta}_n \rangle_m - \overline{\overline{\boldsymbol{\alpha} - \boldsymbol{\alpha}_n}}\chi\boldsymbol{\delta}\right) + \frac{\eta_0}{\Delta t}(\boldsymbol{\alpha} - \tilde{\boldsymbol{\alpha}}_n) : (\boldsymbol{\alpha} - \tilde{\boldsymbol{\alpha}}_n) \\ \Delta J^m(\boldsymbol{\sigma}, \boldsymbol{\alpha}) = \frac{1}{2}\boldsymbol{\sigma} : \mathbb{S}^m : \boldsymbol{\sigma} + \sigma_y(\alpha - \alpha_n)_{eq} - \frac{\eta_0}{\Delta t}(\boldsymbol{\alpha} - \tilde{\boldsymbol{\alpha}}_n) : (\boldsymbol{\alpha} - \tilde{\boldsymbol{\alpha}}_n) \end{cases} \tag{44}$$

where J_0^m is the linearized local incremental potential in the matrix phase.

4.2. Estimation of the effective incremental bi-potential $\Pi_\Delta\left(\bar{\boldsymbol{\varepsilon}},\ \bar{\boldsymbol{\sigma}}_m\right)$

The effective incremental bi-potential of the RVE is determined by calculating the volumetric average of the two terms of the local incremental bi-potential given in Eq. (44):

$$\Pi_\Delta\left(\bar{\boldsymbol{\varepsilon}}, \bar{\boldsymbol{\sigma}}\right) = \inf_{\langle\boldsymbol{\varepsilon}\rangle=\bar{\boldsymbol{\varepsilon}}}\left[f^m\left\langle \inf_{\boldsymbol{\alpha}}\left(J_0^m\left(\boldsymbol{\varepsilon},\boldsymbol{\alpha}\right)+\Delta J^m\left(\boldsymbol{\sigma},\boldsymbol{\alpha}\right)\right)\right\rangle_m+\sum_{r=1}^{N} f^{i,r}\left\langle b_e^{i,r}\left(\boldsymbol{\varepsilon},\boldsymbol{\sigma}\right)\right\rangle_{i,r}\right] \tag{45}$$

The secant function $\eta_{sct}\left(\dot{\alpha}_{eq},\boldsymbol{\sigma}\right)$ of the matrix phase is defined as (Lahellec and Suquet, 2007b):

$$\eta_{sct}\left(\dot{\alpha}_{eq},\boldsymbol{\sigma}\right)=\frac{1}{3\dot{\alpha}_{eq}}\frac{\partial b_p^m}{\partial\dot{\alpha}_{eq}}\left(\boldsymbol{\sigma},\boldsymbol{\alpha}\right)=\frac{\sigma_y}{3\dot{\alpha}_{eq}} \tag{46}$$

and Eq. (45) satisfies

$$\Pi_\Delta^m\left(\bar{\boldsymbol{\varepsilon}}, \bar{\boldsymbol{\sigma}}\right) \leq \inf_{\langle\ \boldsymbol{\varepsilon}\rangle=\bar{\boldsymbol{\varepsilon}}}\left\{f^m\left[\left\langle \inf_{\boldsymbol{\alpha}} J_0^m\left(\boldsymbol{\varepsilon},\boldsymbol{\alpha}\right)\right\rangle_m+\left\langle \sup_{\boldsymbol{\alpha}}\Delta J^m\left(\boldsymbol{\sigma},\boldsymbol{\alpha}\right)\right\rangle_m\right]+\sum_{r=1}^{N} f^{i,r}\left\langle b_e^{i,r}\left(\boldsymbol{\varepsilon},\boldsymbol{\sigma}\right)\right\rangle_{i,r}\right\} \tag{47}$$

Note that the local optimization problem in Eq. (47) is solved with respect to the internal variable $\boldsymbol{\alpha}$ only instead of the set of variables $(\boldsymbol{\alpha},\boldsymbol{\beta})$ as defined in Eq.(37) at every point $\underline{x}\subset\Omega_m$. This largely deduces the complexity of the local optimization problem. The estimate (47) of the effective bi-potential $\Pi_\Delta\left(\bar{\boldsymbol{\varepsilon}}, \bar{\boldsymbol{\sigma}}\right)$ with the non-associated perfectly plastic matrix has the similar form as that pertained to nonlinear viscoelastic composites without hardening studied in Lahellec and Suquet (2007b).

According to previous studies (Castañeda and Willis, 1999, Castañeda, 2002, Lahellec and Suquet, 2007b), sharper estimates of $\Pi_\Delta\left(\bar{\boldsymbol{\varepsilon}}, \bar{\boldsymbol{\sigma}}\right)$ can be obtained by requiring only the stationarity of ΔJ^m instead of its supremum with respect to $\boldsymbol{\alpha}$. Therefore, one gets:

$$\Pi_\Delta\left(\bar{\boldsymbol{\varepsilon}}, \bar{\boldsymbol{\sigma}}\right) \simeq \inf_{\langle\ \boldsymbol{\varepsilon}\rangle=\bar{\boldsymbol{\varepsilon}}}\left\{f^m\left[\left\langle \inf_{\boldsymbol{\alpha}} J_0^m\left(\boldsymbol{\varepsilon},\boldsymbol{\alpha}\right)\right\rangle_m+\left\langle \operatorname{stat}_{\boldsymbol{\alpha}}\Delta J^m\left(\boldsymbol{\sigma},\boldsymbol{\alpha}\right)\right\rangle_m\right]+\sum_{r=1}^{N} f^{i,r}\left\langle b_e^{i,r}\left(\boldsymbol{\varepsilon},\boldsymbol{\sigma}\right)\right\rangle_{i,r}\right\} \tag{48}$$

It is worth noticing that the difference function in the increment potential ΔJ^m is generally non-quadratic. In order to determine the stationarity of ΔJ^m with respect to $\boldsymbol{\alpha}$, we rewrite the plastic bi-potential in the following form:

$$b_p^m\left(\boldsymbol{\sigma},\dot{\boldsymbol{\alpha}}\right)=Y\left(\boldsymbol{\sigma},\frac{\left(\boldsymbol{\alpha}-\boldsymbol{\alpha}_n\right)_{eq}^2}{\Delta t^2}\right) \tag{49}$$

The concavity of Y ensures that $\langle Y\left(\boldsymbol{\sigma},\boldsymbol{a}\right)\rangle_m \leq Y\langle\left(\boldsymbol{\sigma},\boldsymbol{a}\right)\rangle_m$ for any field $\boldsymbol{a}\left(\underline{x}\right)$. One then gets the following order relation:

$$\langle\Delta J^m\left(\boldsymbol{\sigma},\boldsymbol{\alpha}\right)\rangle_m \leq \left\langle\Delta\tilde{J}^m\left(\boldsymbol{\sigma},\boldsymbol{\alpha}\right)\right\rangle_m=\frac{1}{2}\langle\boldsymbol{\sigma}\rangle_m:\mathbb{S}^m:\langle\boldsymbol{\sigma}\rangle_m+\Delta t Y\left(\left\langle\boldsymbol{\sigma},\frac{\left(\boldsymbol{\alpha}-\boldsymbol{\alpha}_n\right)_{eq}^2}{\Delta t^2}\right\rangle_m\right)-\left\langle\frac{\eta_0}{\Delta t}\left(\boldsymbol{\alpha}-\tilde{\boldsymbol{\alpha}}_n\right):\left(\boldsymbol{\alpha}-\tilde{\boldsymbol{\alpha}}_n\right)\right\rangle_m \tag{50}$$

The stationarity of $\left\langle \Delta\tilde{J}^m(\boldsymbol{\sigma},\boldsymbol{\alpha})\right\rangle_m$ with respect to $\boldsymbol{\alpha}$ yields

$$2\eta_p \frac{(\boldsymbol{\alpha}-\boldsymbol{\alpha}_n)}{\Delta t} = 2\eta_0 \frac{(\boldsymbol{\alpha}-\tilde{\boldsymbol{\alpha}}_n)}{\Delta t} \tag{51}$$

The coefficient η_p is the secant viscosity associated with the plastic material without hardening and given by:

$$\eta_p = \eta_{sct}\left(\bar{\bar{\dot{\boldsymbol{\alpha}}}}, \langle\boldsymbol{\sigma}\rangle_m\right) = \frac{\left\langle\sigma_y\right\rangle_m}{3\bar{\bar{\dot{\boldsymbol{\alpha}}}}}, \quad \text{with } \bar{\bar{\dot{\boldsymbol{\alpha}}}} = \sqrt{\frac{2}{3}\langle\dot{\boldsymbol{\alpha}}:\dot{\boldsymbol{\alpha}}\rangle_m} \tag{52}$$

It is noticed that (51) can be rewritten in the following form:

$$\boldsymbol{\alpha}=\frac{\boldsymbol{\alpha}_n-\theta\tilde{\boldsymbol{\alpha}}_n}{1-\theta}, \quad \text{with } \theta = \frac{\eta_0}{\eta_p} \tag{53}$$

With this relation, the last term in (48) can be evaluated and $\Pi_\Delta(\bar{\boldsymbol{\varepsilon}},\bar{\boldsymbol{\sigma}})$ can be further estimated as follows:

$$\Pi_\Delta(\bar{\boldsymbol{\varepsilon}},\bar{\boldsymbol{\sigma}}) \simeq \Pi_0(\bar{\boldsymbol{\varepsilon}}) + \Delta\Pi^m(\bar{\boldsymbol{\sigma}}) \tag{54}$$

with

$$\Pi_0(\bar{\boldsymbol{\varepsilon}}) = \inf_{\langle\boldsymbol{\varepsilon}\rangle=\bar{\boldsymbol{\varepsilon}}}\left[f^m\left\langle\inf_{\boldsymbol{\alpha}} J_0^m(\boldsymbol{\varepsilon},\boldsymbol{\alpha})\right\rangle_m + \frac{1}{2}\sum_{r=1}^{N} f^{i,r}\langle\boldsymbol{\varepsilon}\rangle_{i,r} : \mathbb{C}^{i,r} : \langle\boldsymbol{\varepsilon}\rangle_{i,r}\right] \tag{55a}$$

$$\Delta\Pi^m(\bar{\boldsymbol{\sigma}}) = f^m\left(\frac{1}{2}\langle\boldsymbol{\sigma}\rangle_m : \mathbb{S}^m : \langle\boldsymbol{\sigma}\rangle_m + \left\langle\frac{\eta_p\theta}{\Delta t(\theta-1)}(\boldsymbol{\alpha}_n-\tilde{\boldsymbol{\alpha}}_n):(\boldsymbol{\alpha}_n-\tilde{\boldsymbol{\alpha}}_n)\right\rangle_m\right) + \frac{1}{2}\sum_{r=1}^{N} f^{i,r}\langle\boldsymbol{\sigma}\rangle_{i,r} : \mathbb{S}^{i,r} : \langle\boldsymbol{\sigma}\rangle_{i,r} \tag{55b}$$

By using the stationarity condition of (54) over $\tilde{\boldsymbol{\alpha}}_n$ and θ, one gets:

$$\theta = 1 \pm \sqrt{\frac{\langle(\boldsymbol{\alpha}_n-\tilde{\boldsymbol{\alpha}}_n):(\boldsymbol{\alpha}_n-\tilde{\boldsymbol{\alpha}}_n)\rangle_m}{\langle(\boldsymbol{\alpha}-\tilde{\boldsymbol{\alpha}}_n):(\boldsymbol{\alpha}-\tilde{\boldsymbol{\alpha}}_n)\rangle_m}} \tag{56}$$

$$\tilde{\boldsymbol{\alpha}}_n = \frac{\langle\boldsymbol{\alpha}_n\rangle_m + (\theta-1)\langle\boldsymbol{\alpha}\rangle_m}{\theta} \tag{57}$$

It is noticed that in the aforementioned calculations, the sign '-' is adopted in Eq. (56), which corresponds to solving the problem (47) with an infimum and therefore to a rigorous lower bound for the effective bi-potential Π_Δ.

With the help of minimization of $J_0^m(\boldsymbol{\varepsilon},\boldsymbol{\alpha})$ with respect to $\boldsymbol{\alpha}$, one finally obtains (the detailed calculation is given in Appendix B):

$$\boldsymbol{\alpha} = \left(\mathbb{C}^m + \frac{2\theta\eta}{\Delta t}\mathbb{K}\right)^{-1} : \left[\mathbb{K}:\mathbb{C}^m:\boldsymbol{\varepsilon} + \frac{2\theta\eta}{\Delta t}\tilde{\boldsymbol{\alpha}}_n\right] = d\mathbb{K}:\boldsymbol{\varepsilon}+e\tilde{\boldsymbol{\alpha}}_n \tag{58a}$$

where $d = \frac{\mu}{\frac{\eta\theta}{\Delta t}+\mu}$, $e = \frac{\frac{\eta\theta}{\Delta t}}{\frac{\eta\theta}{\Delta t}+\mu}$. η denotes the uniform total secant viscosity taken at $\bar{\bar{\dot{\boldsymbol{\alpha}}}}$ of the non-associated plastic matrix without hardening:

$$\eta\left(\bar{\bar{\dot{\boldsymbol{\alpha}}}}, \langle\boldsymbol{\sigma}\rangle_m\right) = -\frac{\kappa\left(\langle\sigma_m\rangle_m - c\right)}{\bar{\bar{\dot{\boldsymbol{\alpha}}}}} \tag{59}$$

4.3. *Estimation of the effective potential $\Pi_0(\bar{\boldsymbol{\varepsilon}})$ of homogenized material*

The last step of formulation is the estimation of the effective potential $\Pi_0(\bar{\boldsymbol{\varepsilon}})$ of the homogenized equivalent material (HEM) in order to estimate the macroscopic elastic-plastic behavior of the heterogeneous rocks. This is based on the choice of a thermoelastic linear comparison composite (LCC). Substituting the result found in (58a) for the expression of $J_0^m(\boldsymbol{\varepsilon},\boldsymbol{\alpha})$ in (44) and making use of Eq. (53), one defines the local increment potential $\pi_0^m(\boldsymbol{\varepsilon})$ of the LCC as follows:

$$\pi_0^m(\boldsymbol{\varepsilon}) = \inf_{\boldsymbol{\alpha}} J_0^m(\boldsymbol{\varepsilon},\boldsymbol{\alpha}) = \frac{1}{2}\boldsymbol{\varepsilon} : \mathbb{C}_0^m : \boldsymbol{\varepsilon} + \boldsymbol{\rho}_0^m : \boldsymbol{\varepsilon} + \zeta_0^m \tag{60}$$

The tensors $\mathbb{C}_0^m$ and $\boldsymbol{\rho}_0^m$ as well as the scalar coefficient ζ_0^m are all uniform in the matrix phase and given by:

$$\begin{cases} \mathbb{C}_0^m = 3k^m\mathbb{J} + 2\mu_0^m\mathbb{K}, \quad \text{with } \mu_0^m = (1-d)^2\mu^m + \frac{\theta\eta_p}{\Delta t}d^2 \\ \boldsymbol{\rho}_0^m = 2\left[\frac{\theta\eta_p}{\Delta t}d(e-1) - \mu^m(1-d)\right]\tilde{\boldsymbol{\alpha}}_n - 3k^m\left(\langle\boldsymbol{\beta}_n\rangle_m + \overline{\overline{\boldsymbol{\alpha}-\boldsymbol{\alpha}_n}}\chi\boldsymbol{\delta}\right) \\ \zeta_0^m = \left[e^2\mu^m + \frac{\theta\eta_p}{\Delta t}(e-1)^2\right]\tilde{\boldsymbol{\alpha}}_n : \tilde{\boldsymbol{\alpha}}_n + \frac{9}{2}k^m\left(\langle\beta_n\rangle_m + \overline{\overline{\alpha-\alpha_n}}\chi\right)^2 \end{cases} \tag{61}$$

The quantities θ, $\tilde{\boldsymbol{\alpha}}_n$ and η are defined in Eqs. (56), (57) and (59), respectively. Further, the effective potential $\Pi_0(\bar{\boldsymbol{\varepsilon}})$ defined in Eq. (55a) can be written as

$$\Pi_0(\bar{\boldsymbol{\varepsilon}}) = \frac{1}{2}\bar{\boldsymbol{\varepsilon}} : \bar{\mathbb{C}} : \bar{\boldsymbol{\varepsilon}} + \bar{\boldsymbol{\rho}} : \bar{\boldsymbol{\varepsilon}} + \bar{\zeta} \tag{62}$$

The effective tensors $\bar{\mathbb{C}}$ and $\bar{\boldsymbol{\rho}}$ as well as the scalar variable $\bar{\zeta}$ are expressed in Appendix C.

By using the expression of $\Pi_0(\bar{\boldsymbol{\varepsilon}})$ (Eq. (62)) in (55a), the macroscopic stress tensor $\bar{\boldsymbol{\sigma}}$ of the HEM as that defined in Eq. (41) can be approximated by the following differentiation procedure:

$$\bar{\boldsymbol{\sigma}} = \frac{\partial\Pi_\Delta}{\partial\bar{\boldsymbol{\varepsilon}}}(\bar{\boldsymbol{\varepsilon}},\bar{\boldsymbol{\sigma}}) = \frac{\mathrm{d}\Pi_0}{\mathrm{d}\bar{\boldsymbol{\varepsilon}}}(\bar{\boldsymbol{\varepsilon}}) = f^m\langle\boldsymbol{\sigma}\rangle_m + \sum_{r=1}^{N} f^{i,r}\langle\boldsymbol{\sigma}\rangle_{i,r} \tag{63}$$

with

$$\langle\boldsymbol{\sigma}\rangle_m = \mathbb{C}_0^m : \langle\boldsymbol{\varepsilon}\rangle_m + \boldsymbol{\rho}_0 \tag{64a}$$

$$\langle\boldsymbol{\sigma}\rangle_{i,r} = \mathbb{C}^{i,r} : \langle\boldsymbol{\varepsilon}\rangle_{i,r} \tag{64b}$$

5. Fluctuations of local fields and computational aspects

5.1. *Fluctuations of local fields in matrix*

In order to assess the accuracy of the BIV model, not only the macroscopic responses of the HEM but also the representative fluctuations of local fields should be investigated. In this study, we shall evaluate the fluctuations of local stress and plastic strain fields in the matrix. The fluctuations of interest contain the first- and second-order moments of the these fields. Following Idiart and Castañeda (2007) the quadratic fluctuation of the local stress in the matrix is defined as

$$\mathbb{F}^{m}_{\boldsymbol{\sigma}} \equiv \langle \boldsymbol{\sigma} - \langle \boldsymbol{\sigma} \rangle_m \rangle_m \otimes \langle \boldsymbol{\sigma} - \langle\ \boldsymbol{\sigma} \rangle_m \rangle_m = \langle \boldsymbol{\sigma} \otimes \boldsymbol{\sigma} \rangle_m - \langle\ \boldsymbol{\sigma} \rangle_m \otimes \langle \boldsymbol{\sigma} \rangle_m \tag{65}$$

where $\langle \boldsymbol{\sigma} \rangle_m$ and $\langle \boldsymbol{\sigma} \otimes \boldsymbol{\sigma} \rangle_m$ represent the first and second-order moment of local stress field over the matrix. $\langle \boldsymbol{\sigma} \rangle_m$ can be obtained from the relation (64a). However it is generally difficult to calculate $\langle \boldsymbol{\sigma} \otimes \boldsymbol{\sigma} \rangle_m$. In order to amend this issue, here we adopt the following expression proposed in (Agoras et al., 2016):

$$\sqrt{\mathbb{F}^{m}_{\boldsymbol{\sigma}} :: \mathbb{K}} = \sqrt{\langle \boldsymbol{s} : \boldsymbol{s} \rangle_m - \langle \boldsymbol{s} \rangle_m : \langle \boldsymbol{s} \rangle_m} = \sqrt{\frac{2}{3}\left(\overline{\overline{\sigma}}^2 - \left(\bar{\sigma}^m_{eq}\right)^2\right)} \tag{66}$$

with $\bar{\sigma}^{(m)}_{eq} = \sqrt{\frac{3}{2} \langle \boldsymbol{s} \rangle_m : \langle \boldsymbol{s} \rangle_m}$ and $\overline{\overline{\sigma}} = \sqrt{\frac{3}{2} \langle \boldsymbol{s} : \boldsymbol{s} \rangle_m}$ for the evaluation of $\langle \boldsymbol{s} \rangle_m$ and $\langle \boldsymbol{s} : \boldsymbol{s} \rangle_m$. Together with Eq. (B.9), one further obtains

$$\overline{\overline{\sigma}} = 3\eta \overline{\overline{\dot{\alpha}}} \tag{67}$$

The calculation of the denominator $\overline{\overline{\dot{\alpha}}}$ is given in Section 5.3. One can notice that it is easy to obtain the fluctuation of local stress field (66) with the help of Eqs. (64a) and (67).

Similarly, the fluctuation of the local plastic strain field in the matrix is defined as:

$$\mathbb{F}^{m}_{\boldsymbol{\varepsilon}^p} \equiv \langle \boldsymbol{\varepsilon}^p - \langle \boldsymbol{\varepsilon}^p \rangle_m \rangle_m \otimes \langle\ \boldsymbol{\varepsilon}^p - \langle \boldsymbol{\varepsilon}^p \rangle_m \rangle_m = \langle \boldsymbol{\varepsilon}^p \otimes \boldsymbol{\varepsilon}^p \rangle_m - \langle\ \boldsymbol{\varepsilon}^p \rangle_m \otimes \langle\ \boldsymbol{\varepsilon}^p \rangle_m \tag{68}$$

where $\langle \boldsymbol{\varepsilon}^p \rangle_m$ and $\langle \boldsymbol{\varepsilon}^p \otimes \boldsymbol{\varepsilon}^p \rangle_m$ represent the first and second-order moments of local plastic strain field over the matrix. For the ease of calculation, we provide the result for the standard derivation of the plastic strain filed in the matrix phase, that is:

$$\sqrt{\mathbb{F}^{m}_{\boldsymbol{\varepsilon}^p} :: \mathbb{K}} = \sqrt{\langle \boldsymbol{\alpha} : \boldsymbol{\alpha} \rangle_m - \langle \boldsymbol{\alpha} \rangle_m : \langle \boldsymbol{\alpha} \rangle_m} = \sqrt{\frac{3}{2}\left(\overline{\overline{\alpha}}^2 - \left(\bar{\alpha}^m_{eq}\right)^2\right)} \tag{69}$$

with $\bar{\alpha}^{m}_{eq} = \sqrt{\frac{2}{3} \langle \boldsymbol{\alpha} \rangle_m : \langle \boldsymbol{\alpha} \rangle_m}$ and $\overline{\overline{\alpha}} = \sqrt{\frac{2}{3} \langle \boldsymbol{\alpha} : \boldsymbol{\alpha} \rangle_m}$, being the first- and second-order moment of $\boldsymbol{\alpha}$.

5.2. *Computation of the first and second-order moment of* $\boldsymbol{\alpha}$

The calculation of θ, $\tilde{\boldsymbol{\alpha}}_n$ and $\sqrt{\mathbb{F}^{m}_{\boldsymbol{\varepsilon}^p} :: \mathbb{K}}$ from Eqs.(56), (57) and (69) needs the determination of the first- and second-order moment of $\boldsymbol{\alpha}$ in the plastic matrix. The first moment is given by:

$$\langle \boldsymbol{\alpha} \rangle_m = \langle d\mathbb{K} : \boldsymbol{\varepsilon} + e\tilde{\boldsymbol{\alpha}}_n \rangle_m \tag{70}$$

Since the quantities d, e and $\tilde{\boldsymbol{\alpha}}_n$ are uniform in the matrix phase, one thus obtains

$$\langle \boldsymbol{\alpha} \rangle_m = d\mathbb{K} : \langle \boldsymbol{\varepsilon} \rangle_m + e : \tilde{\boldsymbol{\alpha}}_n \tag{71}$$

Similarly, the second-order moment of $\boldsymbol{\alpha}$ is calculated by:

$$\langle \boldsymbol{\alpha} : \boldsymbol{\alpha} \rangle_m = d^2 \mathbb{K} :: \langle \boldsymbol{\varepsilon} \otimes \boldsymbol{\varepsilon} \rangle_m + 2de\tilde{\boldsymbol{\alpha}}_n : \langle \boldsymbol{\varepsilon} \rangle_m + e^2 \tilde{\boldsymbol{\alpha}}_n : \tilde{\boldsymbol{\alpha}}_n \tag{72}$$

The first and second terms at the right hand side of Eq. (72) are related to the second- and first-order moments of $\boldsymbol{\varepsilon}$ in the matrix phase and can be obtained from Eqs.(C.6) and (C.3), respectively.

5.3. Computation of the second-order moment of $\dot{\boldsymbol{\alpha}}$

To calculate η from Eq. (59), the denominator $\bar{\bar{\dot{\boldsymbol{\alpha}}}}$ related to the second-order moment of $\dot{\boldsymbol{\alpha}}$ should be first determined by:

$$\bar{\bar{\dot{\boldsymbol{\alpha}}}} = \sqrt{\frac{2}{3} \langle \dot{\boldsymbol{\alpha}} : \dot{\boldsymbol{\alpha}} \rangle_m} = \frac{1}{\Delta t} \sqrt{\frac{2}{3} \langle (\boldsymbol{\alpha} - \boldsymbol{\alpha}_n) : (\boldsymbol{\alpha} - \boldsymbol{\alpha}_n) \rangle_m} \tag{73}$$

It is noticed that it is generally difficult to calculate $\langle (\boldsymbol{\alpha} - \boldsymbol{\alpha}_n) : (\boldsymbol{\alpha} - \boldsymbol{\alpha}_n) \rangle_m$ due to the inaccessibility of the term $\langle \boldsymbol{\alpha} : \boldsymbol{\alpha}_n \rangle_m$. However, thanks to Eq. (57), $\bar{\bar{\dot{\boldsymbol{\alpha}}}}$ can be alternatively calculated by the following relation when $\theta \neq 1$:

$$\begin{aligned} \bar{\bar{\dot{\boldsymbol{\alpha}}}} &= \left[\frac{\theta}{\Delta t (1 - \theta)} \right] \sqrt{\frac{2}{3} \langle (\boldsymbol{\alpha}_n - \tilde{\boldsymbol{\alpha}}_n) : (\boldsymbol{\alpha}_n - \tilde{\boldsymbol{\alpha}}_n) \rangle_m} \\ &= \left[\frac{\theta}{\Delta t (1 - \theta)} \right] \sqrt{\frac{2}{3} \left(\langle \boldsymbol{\alpha}_n : \boldsymbol{\alpha}_n \rangle_m - 2 \langle \boldsymbol{\alpha}_n \rangle_m : \tilde{\boldsymbol{\alpha}}_n + \tilde{\boldsymbol{\alpha}}_n : \tilde{\boldsymbol{\alpha}}_n \right)} \end{aligned} \tag{74}$$

where the first- and second-order moments of $\boldsymbol{\alpha}$ are already determined from (71) and (72) respectively.

6. Implementation and numerical assessment of the BIV model

6.1. Local implementation algorithm of BIV model

The numerical implantation algorithm of the proposed BIV model is now presented. This algorithm is developed as a user-defined subroutine for the determination of mechanical behavior of a macroscopic material point in a standard computation code. The material point is subjected to a macroscopic strain increment $\Delta\bar{\boldsymbol{\varepsilon}}$ ($\Delta\bar{\boldsymbol{\varepsilon}} = \dot{\bar{\boldsymbol{\varepsilon}}}\Delta t$) such that $\bar{\boldsymbol{\varepsilon}}_{n+1} = \bar{\boldsymbol{\varepsilon}}_n + \Delta\bar{\boldsymbol{\varepsilon}}$ at t_{n+1}. The numerical algorithm is here used to calculate the macroscopic stress increment using the proposed BIV model. The flowchart of the computational procedure is summarized in Algorithm 1:

Algorithm 1: Flowchart of the local implementation algorithm of BIV

Input: $\dot{\bar{\varepsilon}}, \Delta t, \bar{\sigma}_n, \bar{\varepsilon}_n, \langle \alpha_n \rangle_m, \langle \beta_n \rangle_m, \langle \alpha_n : \alpha_n \rangle_m, \theta_n, \eta_n$

Output: $\bar{\sigma}_{n+1}, \bar{\varepsilon}_{n+1}, \langle \alpha_{n+1} \rangle_m, \langle \beta_{n+1} \rangle_m, \langle \alpha_{n+1} : \alpha_{n+1} \rangle_m, \theta_{n+1}, \eta_{n+1}$

$\bar{\varepsilon}_{n+1} = \bar{\varepsilon}_n + \dot{\bar{\varepsilon}} \Delta t,$

Initialize $\eta_{n+1} = \eta_n, \theta_{n+1} = \theta_n$

Calculate $\mathbb{A}^m_{n+1}, \mathbb{A}^{i,r}_{n+1}, \boldsymbol{a}^m_{n+1}, \boldsymbol{a}^{i,r}_{n+1}, \mathbb{C}^m_{0,n+1}, \boldsymbol{\rho}^m_{0n+1},$

Calculate first order moment of strain field $\langle \varepsilon_{n+1} \rangle^{trial}_m = \mathbb{A}^m_{n+1} : \bar{\varepsilon} + \boldsymbol{a}^m_{n+1},$
$\langle \varepsilon_{n+1} \rangle^{trial}_{i,r} = \mathbb{A}^{i,r}_{n+1} : \bar{\varepsilon} + \boldsymbol{a}^{i,r}_{n+1},$

Elastic prediction: $\langle \sigma_{n+1} \rangle^{trial}_m = \mathbb{C}^m : (\langle \varepsilon_{n+1} \rangle^{trial}_m - \langle \alpha_n \rangle_m - \langle \beta_n \rangle_m)$

if $f(\langle \sigma_{n+1} \rangle^{trial}_m) < 0$ **then**

  $\langle \varepsilon_{n+1} \rangle_m = \langle \varepsilon_{n+1} \rangle^{trial}_m ; \langle \varepsilon_{n+1} \rangle_{i,r} = \langle \varepsilon_{n+1} \rangle^{trial}_{i,r} \quad \langle \alpha_{n+1} \rangle_m = \mathbf{0}; \langle \beta_{n+1} \rangle_m = \mathbf{0}; \langle \alpha_{n+1} : \alpha_{n+1} \rangle_m = 0$

else

  (For clarity, the subscript n+1 will be omitted in the for loop)

  for $j = 1 \ldots m_{iter}$, **do**

    Calculate $\mathbb{C}^m_{0,j}, \boldsymbol{\rho}^m_{0,j}, \varsigma^m_{0,j}$ and $\bar{\mathbb{C}}_j$ with Eqs. (61) and (C.2a)

    Calculate $\mathbb{A}^m_j, \mathbb{A}^{i,r}_j, \boldsymbol{a}^m_j, \boldsymbol{a}^{i,r}_j$ (with Eq.(C.7) for two-phases composite).

    Calculate first moment of strain field $\langle \varepsilon \rangle_{m,j} = \mathbb{A}^m_j : \bar{\varepsilon} + \boldsymbol{a}^m_j$ and $\langle \varepsilon \rangle_{i,r,j} = \mathbb{A}^{i,r}_j : \bar{\varepsilon} + \boldsymbol{a}^{i,r}_j$ with Eqs.(C.3) and (C.4) ;

    Calculate $\langle \sigma \rangle_{m,j}$ and $\langle \sigma \rangle_{i,r,j}$ by using Eq.(64);

    Calculate effective internal variable $\tilde{\alpha}_{n,j}$ and $\langle \alpha \rangle_{m,j}$ with Eqs.(57) and (71);

    Calculate second moment of strain field $\mathbb{K} :: \langle \varepsilon \otimes \varepsilon \rangle_{m,j}$ and $\langle \alpha : \alpha \rangle_{m,j}$ with Eqs.(C.6) and (72);

    Calculate $\overline{\overline{\alpha}}_j$ and $\langle \beta \rangle_j$ with Eqs.(74) and (A.1)

    Calculate θ_j and η_j with Eqs.(56) and (59);

    if $\frac{|\delta\theta_j|}{\theta_j} < \epsilon$ *and* $\frac{|\delta\eta_j|}{\eta_j} < \epsilon$, **then**

      Return;

    else

      $j = j + 1$

  $\bar{\sigma}_{n+1} = \langle \sigma_{n+1} \rangle = f^m \langle \sigma_{n+1} \rangle_m + \sum_{r=1}^{N} f^{i,r} \langle \sigma_{n+1} \rangle_{i,r};$

6.2. Comparisons with direct FEM simulations

The purpose of this section is to verify the accuracy of the BIV model by comparing its prediction with the reference solutions obtained by direct finite element method (FEM) simulations on the unit cell for two kinds of materials. The first one is a composite material with a non-associated Drucker-Prager plastic matrix and elastic inclusions (Figure 3(b)), while the second one is a porous material with non-associated Drucker-Prager plastic matrix and pores. In this section and section 7, the effective properties of the LCC as well as the field fluctuations are evaluated by using the Hashin-Shtrikman bounds, i.e., the HS lower bound for the inclusion-reinforced material and the upper bound for the porous material, more details are given in Appendix C. The microstructure of studied materials is represented by a periodic assembly of 3D unit cells with spherical inclusion or pore. Taking advantage of axial symmetry, the actual hexagonal unit cell is simplified in to a cylinder one and only half an axial symmetry plain is considered in the finite element calculations, as illustrated in Figure 3. FEM computations are performed using ABAQUS 6.14 using quadratic CAX6 elements for inclusion phase and CAX8 elements for matrix phase. Since the focus here is on the modelling of non-associated plastic matrix, we assume the interfaces between the inclusions and matrix are perfect for the inclusion-reinforced material, implying the interface effects are not taken into account here. Note that FEM predictions are labeled "FEM" in the figures. The first- and second-order moments of the local fields are computed from direct volume averaging of the local fields in the unit cell (Yan et al., 2007).

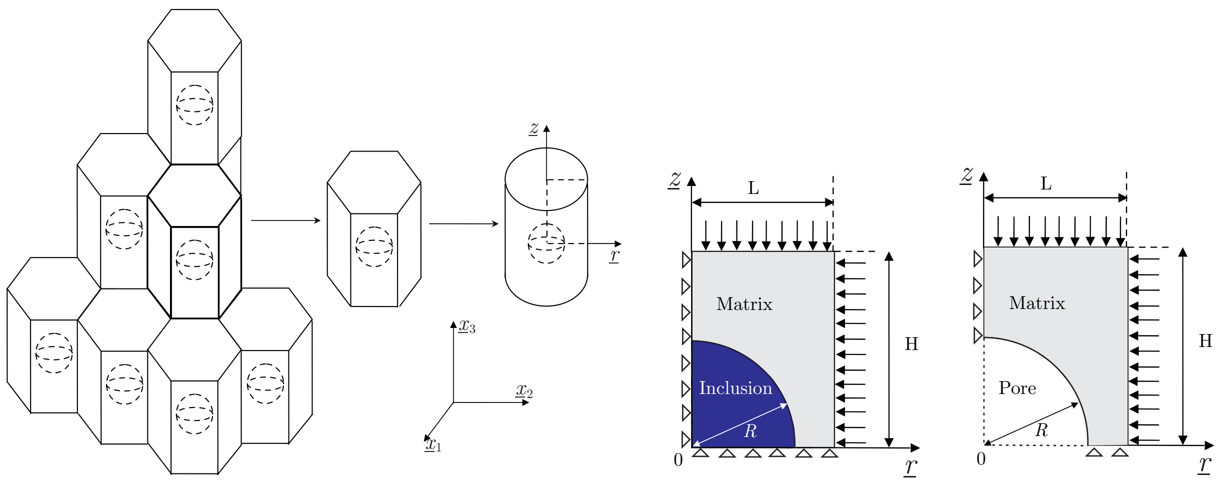

(a) Approximation of 3D hexagonal periodic array material (b) Inclusion-reinforced material (c) porous material

Figure 3: Approximation of 3D hexagonal periodic array with spherical inclusion/pore by axi-symmetric cylinder unit cell

For the inclusion-reinforced material, the input parameters for each constituent phase are listed in Tables 1 and 2. Uniaxial and triaxial compression tests are investigated. The unit cell is first subjected to a confining stress (or hydrostatic stress) and then to a differential stress by increasing the axial strain in the z direction. During the differential stress stage, the lateral displacement $\bar{U}_2$ is kept uniform along the boundary to satisfy the uniform strain boundary condition. The boundary conditions are illustrated in Figure 3(b) and summarized as follows

$$\begin{cases} U_3(r,H) = \bar{U}_3, & 0 < r < L \\ U_2(L,z) = \bar{U}_2, & 0 < z < H \\ U_3(r,0) = 0, & 0 < r < L \\ U_2(0,z) = 0, & 0 < z < H \end{cases} \tag{75}$$

Table 1: Parameters of solid matrix for composite

E^m (MPa)	ν^m	κ	c(MPa)	χ_m
3000	0.3	0.227	30	0.083

Table 2: Parameters of elastic inclusion

E^i (MPa)	ν^i
98000	0.15

The parameters for the matrix phase in the porous material are the same as those for the inclusion-reinforce composite and listed in Table 1. The boundary conditions on the unit cell are given below and illustrated in Figure 3(c).

$$\begin{cases} U_3(r,H) = \bar{U}_3, & 0 < r < L \\ U_2(L,z) = \bar{U}_2, & 0 < z < H \\ U_3(r,0) = 0, & R < r < L \\ U_2(0,z) = 0, & R < z < H \end{cases} \tag{76}$$

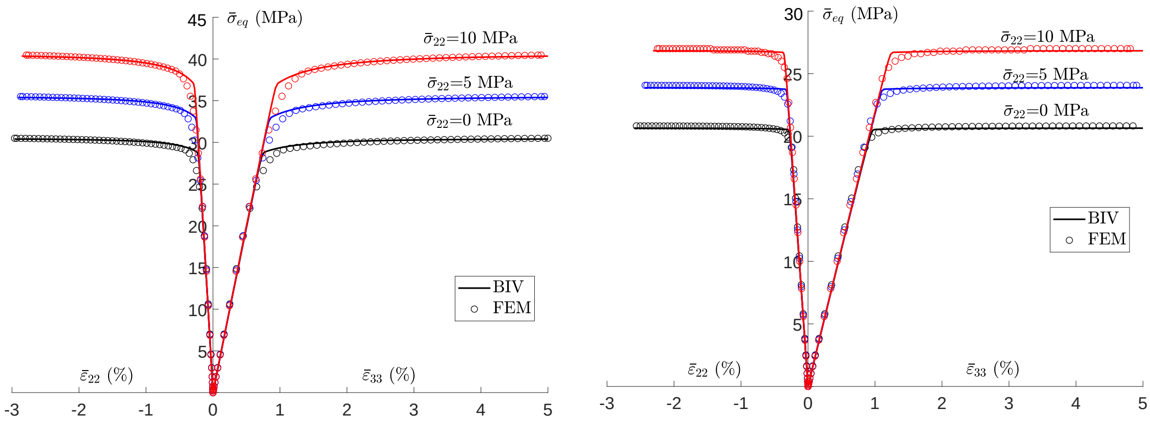

(a) Inclusion-reinforced material (b) Porous material

Figure 4: Macroscopic stress-strain curves for two kinds of heterogeneous materials with non-associated Drucker-Prager perfectly plastic matrix and inclusions/pores (f^i = 15%) in triaxial compression tests with different confining stresses

In Figure 4, one shows the macroscopic stress-strain curves for both the inclusion-reinforced composite and porous material under uniaxial and triaxial compression tests with different confining stresses, respectively obtained by the proposed BIV model and the direct finite element simulations. One can observe that the model's predictions coincide very well with the FEM solutions for the all cases considered.

An example of uniaxial compression test with an unloading-reloading cycle is also studied for the inclusion-reinforced composite with $f^i = 15\%$. The obtained results are presented in Figure 5. One can see the BIV model well reproduces the results given by the FEM simulations.

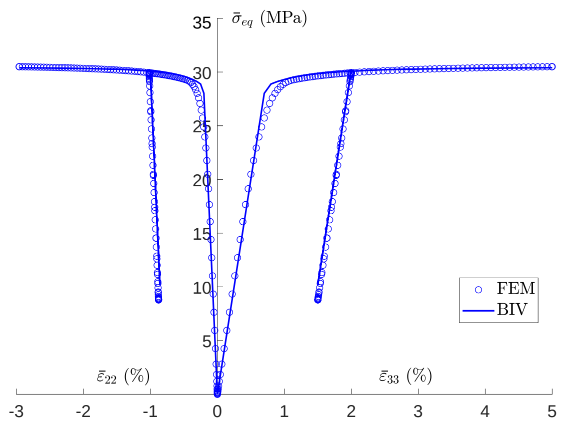

Figure 5: Macroscopic stress-strain curves in uniaxial compression test with an unloading-reloading cycle for the inclusion-reinforced composite with a volume fraction of inclusion of $f^i = 15\%$

7. Extension to rocks with isotropic plastic hardening

As mentioned that ductile and porous rocks usually exhibit plastic hardening. In the case of materials considered here, the plastic hardening occurs in the matrix phase. In the context of a Drucker-Prager plastic criterion, the plastic hardening may leads to an increase of the internal friction coefficient and hydrostatic tensile strength (related to internal cohesion). However, due to the strong dissymmetry of strength between compression and tension in most rocks, the tensile strength is generally small and not affected by the plastic deformation process. The plastic hardening generally enhances the shear strength through the evolution of the internal frictional coefficient. Therefore, with the assumption of an isotropic plastic hardening, the internal frictional coefficient of the matrix κ is here assumed to increase during plastic process according to the following law:

$$\kappa(\gamma^p) = \kappa_m - (\kappa_m - \kappa_0)\, e^{-b_1 \gamma^p} \tag{77}$$

where κ_0 and κ_m denote the initial threshold and the asymptotic value of the frictional coefficient respectively, while b_1 is a parameter controlling the plastic hardening rate.

On the other hand, the plastic dilatancy coefficient χ can also evolve with the plastic deformation history, translating the transition from plastic compressibility to dilatancy. Therefore, we here consider that χ is also a function of γ^p through the following relation

$$\chi(\gamma^p) = \chi_m(1 - e^{-b_2 \gamma^p}) \tag{78}$$

where χ_m is the asymptotic value of the plastic dilatancy coefficient, and b_2 is a parameter controlling its evolution.

In order to fully account for this kind of plastic hardening law in the proposed BIV model, the thermodynamics formulation presented above should be modified by considering the evolution of elastic domain during plastic deformation process. However, due to the fact that the plastic hardening is described by the evolution of the friction coefficient, the evolution measurement of elastic domain cannot be represented by a constant force variable but by a function of mean stress. This render the mathematical treatment of the BIV model very complicated. In order to avoid this complex mathematical difficulty and provide a pragmatical model being easy to be implemented, we shall propose a heuristic extension of the BIV model formulated above for materials without plastic hardening. According to the theoretical formulation presented in Sections 3 and 4, when the values κ, c and χ are constant, the average secant viscosity function of solid matrix η is given in Eq.(59). We here assume that this result remains applicable for the solid matrix where the values of κ and χ are step by step updated at each loading increment. Therefore, we propose an explicit incremental hardening scheme. The average secant viscosity function and the plastic dilatancy coefficient χ at the loading increment $n+1$ is approximated as follows (for the sake of simplicity, the increment number $n+1$ is omitted in the following equations):

$$\eta = -\frac{\kappa\left(\langle \gamma_n^p \rangle_m\right)\left(\langle \sigma_m \rangle_m - c\right)}{\overline{\overline{\dot{\alpha}}}} \tag{79}$$

$$\chi\left(\langle \gamma_n^p \rangle_m\right) = \chi_m (1 - e^{-b_2 \langle \gamma_n^p \rangle_m}) \tag{80}$$

In these relations, $\langle \gamma_n^p \rangle_m$ is the average value of equivalent plastic shear strain in the solid matrix γ^p calculated by Eq.(A.2) at the end of the loading increment n and its value if frozen during the current increment $n+1$. Accordingly, the values of frictional coefficient κ and plastic dilatancy coefficient χ are also frozen to those calculated at the end of the previous increment such as $\kappa\left(\langle \gamma_n^p \rangle_m\right)$ and $\chi\left(\langle \gamma_n^p \rangle_m\right)$. Therefore, the solid matrix is treated as a perfectly plastic material during the current loading increment.

7.1. *Comparisons with direct FEM simulations*

The accuracy of the heuristically extended BIV model for materials with an isotropic hardening is now checked by comparing the model's predictions with direct FEM simulations for both local and macroscopic responses. Two kinds of materials are again studied: inclusion-reinforced composites and porous materials. Conventional triaxial compression tests are considered. The boundary conditions for the two materials are the same as those presented in Section 6.2. The following input parameters are selected for the isotropic hardening law: $\kappa_0 = 1 \times 10^{-5}$, $\kappa_m = 0.227$, $b_1 = 140$, $\chi_m = 0.083$ and $b_2 = 70$.

7.1.1. *Inclusion-reinforced composites*

Two volume fractions of elastic inclusions are considered: $f^i = 5\%$ and $f^i = 15\%$. In Figure 6, one shows the macroscopic stress-strain curves in the uniaxial compression test, respectively obtained by the BIV model and FEM simulations. It can be seen that there is a good agreement between these two results. In Figure 7, we emphasize the volume strain evolution $\bar{\varepsilon}_v$ as a function of axial strain $\bar{\varepsilon}_{33}$ with different values of the maximum dilatancy coefficient χ_m and for $f^i = 15\%$. It is noticed that the proposed BIV model is able to well reproduce the volume compressibility-dilatancy transition which is an important property of rocks. More precisely, the volumetric dilatancy is enhanced when the value of χ_m increases. The results due to the BIV model well coincident with the FEM simulations.

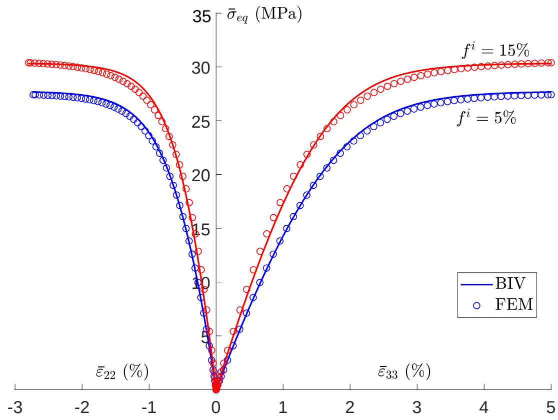

Figure 6: Macroscopic stress-strain curves in uniaxial compression test for an inclusion-reinforced composite with two volume fractions of inclusions ($f^i = 5\%$ and $f^i = 15\%$)

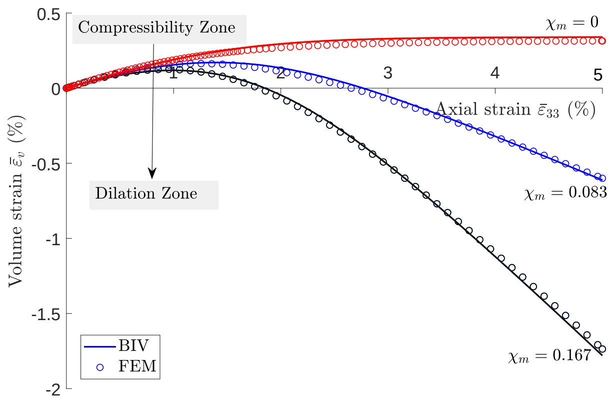

Figure 7: Evolution of macroscopic volumetric strain in uniaxial compression test for different values of plastic dilatancy coefficient χ for an inclusion-reinforced composite with a volume fraction of inclusions of $f^i = 15\%$

Moreover, the proposed BIV model is also able to capture another important property of geological materials, which is the influence of confining stress on the macroscopic behavior. This is clearly illustrated in Figure 8. The stress-strain curves are presented for the uniaxial compression test and two triaxial compression tests respectively with a different confining stress of 10MPa and 20MPa. Again, the BIV predictions are in good agreement with the FEM solutions.

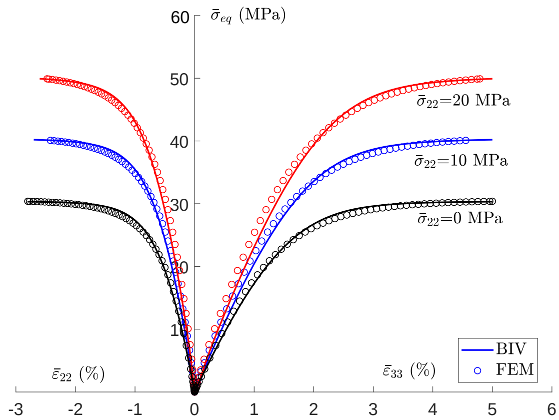

Figure 8: Macroscopic stress-strain curves in uniaxial and triaxial compression tests with two different confining stresses two for an inclusion-reinforced composite with $c^{(2)} = 15\%$

In order to further assess the accuracy of the BIV model, the evolution of local stresses during the loading history is also investigated for the case of uniaxial compression test and of an inclusion volume fraction of $f^i = 15\%$. For instance, the evolutions of average stress respectively in the inclusion and matrix phases are presented in Figure 9(a). In Figure 9(b), one presents the evolutions of the different denominators $\bar{\sigma}^m_{eq}$ and $\overline{\overline{\boldsymbol{\sigma}}}$, respectively related to the first-order and second-order moments of the local stress field over the plastic matrix. Lastly, in Figure 9(c), the evolution of the stress fluctuation $\sqrt{\mathbb{F}^m_{\sigma} :: \mathbb{K}}$ in the matrix is presented. It is observed that the BIV model provides an accurate prediction for the evolution of average stress within the matrix, while a less accurate prediction regarding the average stress in the inclusion phase (Figure 9(a)). The BIV results are also in good agreement with the FEM solutions for the stress moments $\bar{\sigma}^m_{eq}$ and $\overline{\overline{\boldsymbol{\sigma}}}$ (Figure 9(b)). Lastly, although the BIV model overestimates the stress fluctuation within the matrix, it is still able to reproduce the good evolution trend of FEM solutions (Figure 9(c)).

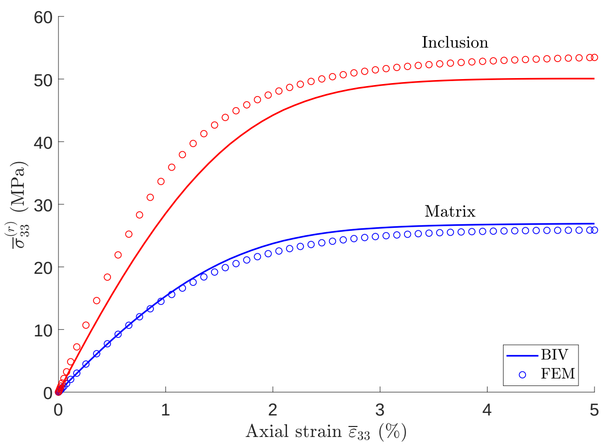

(a) Evolution of average stress in constituent phases versus macroscopic axial strain

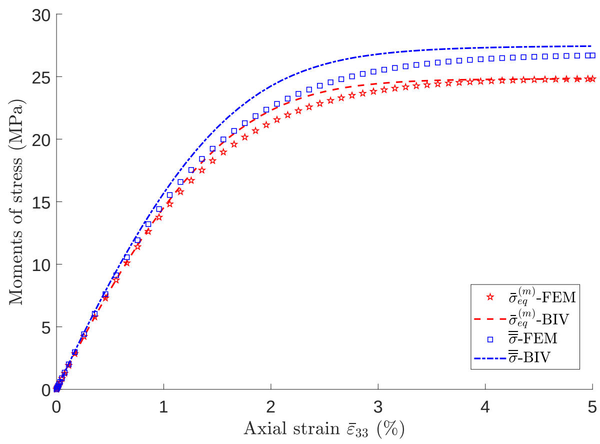

(b) First and second moments of stress over matrix

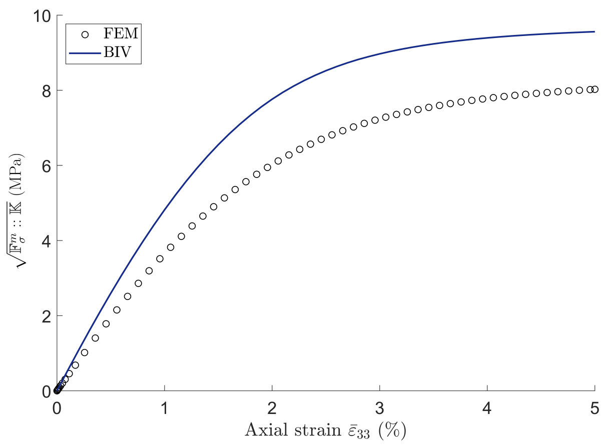

(c) Fluctuations of stress over matrix

Figure 9: Local stress responses in uniaxial compression test for an inclusion-reinforced composite with $f^i = 15\%$

On the other hand, the evolution of the local plastic strain is also studied. In Figure 10(a), one can find a quite good agreement between the BIV result and FEM solution for the first-order moment of local plastic strain field over the matrix $\bar{\alpha}^m_{eq}$. However, it seems that the BIV model underestimates the second-order moment of plastic strain in the matrix $\overline{\overline{\alpha}}$. The fluctuation of plastic strain field is shown in Figure 10(b). The BIV model is able to capture the trend of the FEM solution although there exist some scatters between them.

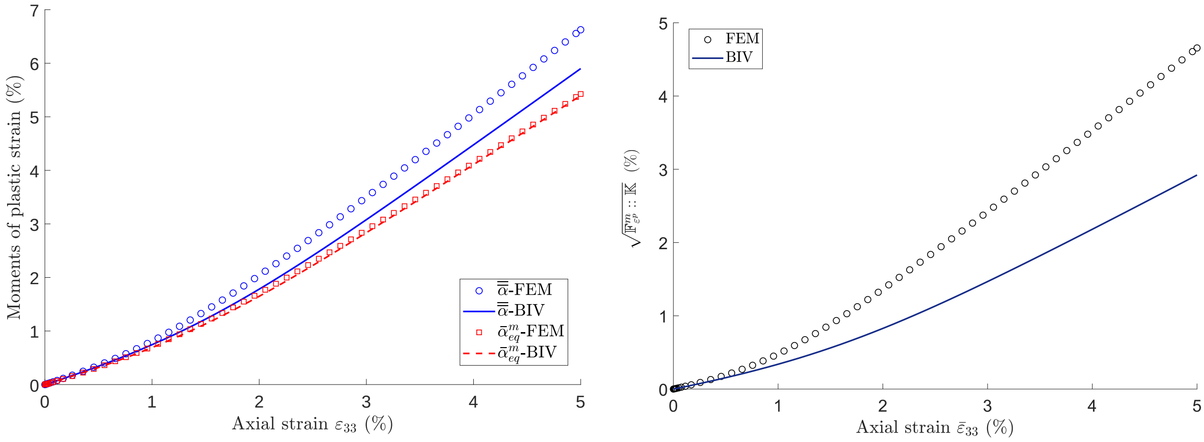

(a) First and second moments of plastic strain over matrix

(b) Fluctuation of plastic strain over matrix

Figure 10: Local plastic strain responses in uniaxial compression test of an inclusion-reinforced composite with $f^i = 15\%$

7.1.2. *Porous material*

The macroscopic stress-strain curves in uniaxial compression test with two values of porosity f^i = 15% and 5% are presented in Figure 11. There is a good agreement between the BIV predictions and FEM results. Furthermore, the stress-strain curves in triaxial compression tests with three different confining stresses are presented in Figure 12 for a porosity of $f^i = 15\%$. Once more, the BIV model correctly captures the effect of confining stress and well reproduces the FEM solutions.

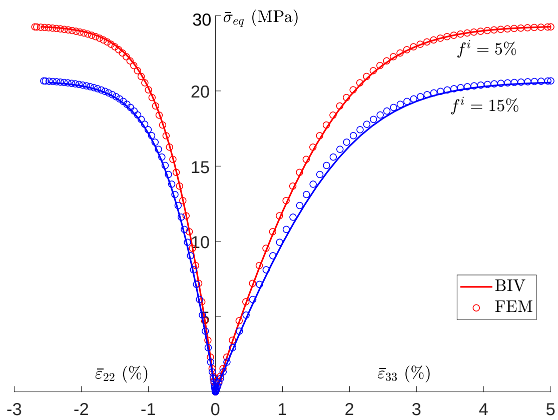

Figure 11: Macroscopic stress-strain curves in uniaxial compression test for a porous material with two different values of porosity ($f^i = 5\%$ and $f^i = 15\%$)

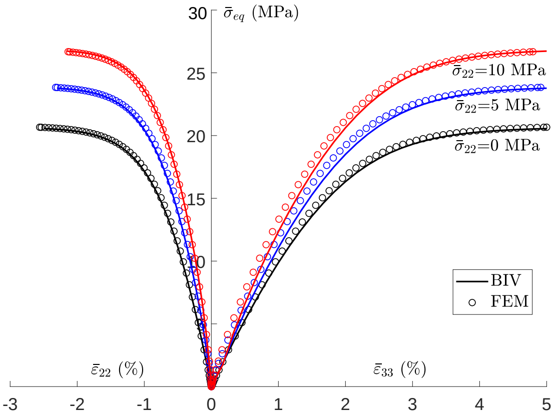

Figure 12: Macroscopic stress-strain curves in triaxial compression tests with three different confining stresses for a porous material with a porosity of $f^i = 15\%$

As for the inclusion-reinforced composite, the local stress and strain responses of porous material are also investigated for the case of uniaxial compression test and with a porosity of $f^i = 15\%$. In Figure 13(a), the evolutions of the first and second-order moments of local stress field over the matrix, $\bar{\sigma}^m_{eq}$ and $\overline{\overline{\sigma}}$, are depicted. The evolution of the stress fluctuations is given in Figure 13(b). One can find a similar trend as that already obtained in Figure 9 for the inclusion-reinforced composite. The evolutions of the moments and fluctuations of local plastic strain field over the matrix are shown in Figure 14. As shown in Figure 14(a), although the BIV model qualitatively reproduces the trend of the FEM solutions, it slightly underestimates the denominators $\bar{\alpha}^m_{eq}$ and $\overline{\overline{\alpha}}$. Compared with Figures 14(b) and 10(b), the fluctuations of the plastic strain field are now better captured by the BIV model for the porous material than for the inclusion-reinforced composite.

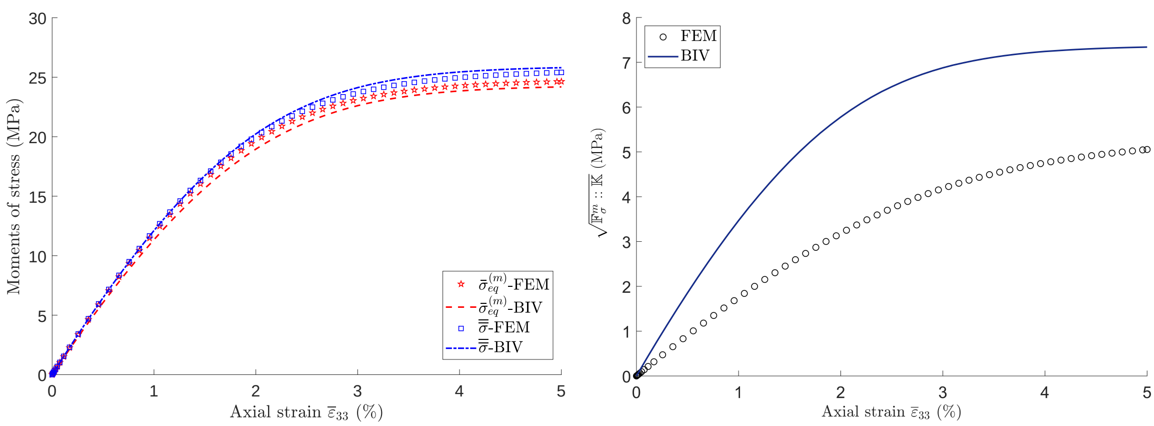

(a) First- and second-order moments of stress over matrix

(b) Fluctuations of stress over matrix

Figure 13: Local stress responses in uniaxial compression test for a porous material with a porosity $f^i = 15\%$

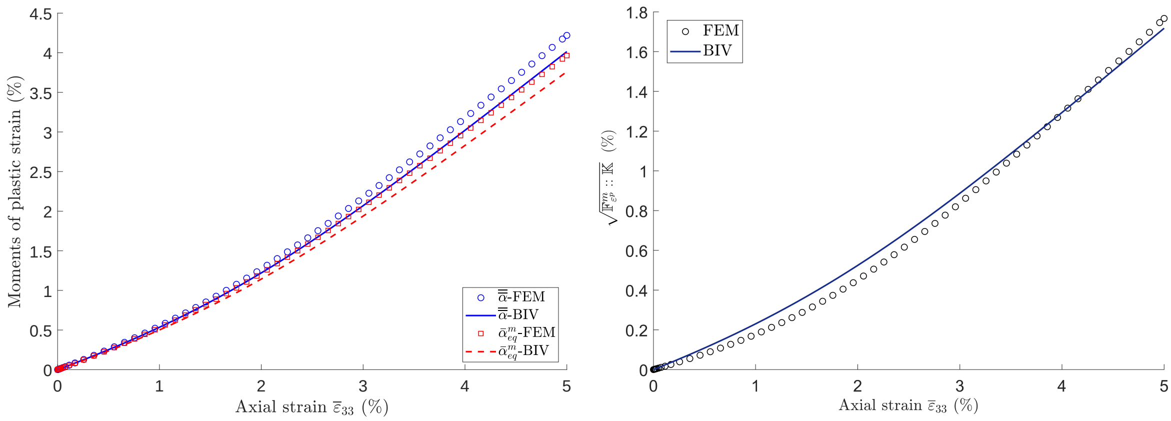

(a) First and second-order moments of plastic strain over matrix

(b) Fluctuations of plastic strain over matrix

Figure 14: Local plastic strain responses in uniaxial compression test for a porous material with a porosity of $f^i = 15\%$

7.2. Application examples

In this section, two application examples are presented to show the ability of the extended bi-potential based incremental variational model to reproduce experimental responses of two typical rocks: the Callovo-Oxfordian claystone and Vosges sandstone.

7.2.1. Application to Callovo-Oxfordian claystone

The Callovo-Oxfordian claystone has been extensively investigated in France as a potential geological barrier for the underground disposal of nuclear waste (Armand et al., 2016). It is a sedimentary rock with complex multi-scale structures (Robinet, 2008). At the micrometer scale, this clayey rock is composed of a quasi-continuous clay matrix in which mineral grains, mainly quartz and calcite grains, are embedded. The clay matrix can exhibit important plastic deformation (Guéry et al., 2008, 2010). For the sake of simplicity, the behavior of clay matrix is here described by an isotropic elastic-plastic model. The linear Drucker-Prager criterion is adopted together with an isotropic hardening law and a non-associated plastic flow rule. On the other hand, for the range of stresses considered in the application, the mechanical behavior of the quartz and calcite grains can be reasonably described by a linear elastic model. Furthermore, as the elastic properties of calcite and quartz are quite similar, for the sake of simplicity, they are seen a single phase of elastic inclusions.

The preliminary challenge of the application of the micro-mechanical model is the identification of local parameters for each constituent phase. To this end, the local mechanical behavior should be determined. This direct identification method is so far not possible because relevant data on mechanical responses at the microscopic scale are not fully available. Here an indirect identification procedure is employed here. The elastic coefficients of the effective elastic inclusion phase are taken as the volumetric average values of the quartz and calcite grains (Jiang et al., 2009). Note that the elastic coefficients of quartz and calcite grains elastic properties of calcite and quartz grains are well known and can be obtained from existing data(Lide, 2004). It is easily to obtain the Young's modulus and Poisson's ratio of the effective elastic inclusion are equal to $E^i = 98\text{GPa}$ and $\nu^i = 0.15$. However, the elastic coefficients of the clay matrix are not available from direct experimental measurement. They are calibrated here by an inverse homogenization procedure (Guéry et al., 2008), from the macroscopic elastic coefficients obtained in triaxial compression tests on the samples with known mineralogical compositions (Chiarelli, 2000). We calculate the typical values of Young's modulus $E^m = 3\text{GPa}$ and Poisson's ratio $\nu^m = 0.3$. On the other hand, the values of plastic parameters of clay matrix are fitted by a numerical optimization of macroscopic stress-strain curves obtained by convention laboratory tests (conventional triaxial compression tests, proportional compression tests, lateral extension test, etc.) for a chosen mineralogical composition similar to that proposed in (Guéry et al., 2008, Shen et al., 2012). The obtained values are then fixed and applied to samples with different mineralogical compositions. The obtained plastic parameters values are given as: $\kappa_0 = 10^{-5}$, $\kappa_m = 0.283$, $b_1 = 250$, $\chi_m = 0.05$, $b_2 = 50$, $c = 20\text{MPa}$.

The mechanical responses of the claystone are now studied using the proposed BIV model in triaxial compression tests, proportional compression tests and lateral extension tests. It is noteworthy that these tests were performed on samples coming from different geological depths ranging from 415.4m to 482.4m, with different mineral compositions. However, a sole set of parameters is used for the modeling of different tests on different samples.

In Figure 15, the stress-strain curves of claystone in triaxial compression tests are presented. One observes a good agreement between model's predictions and experimental data. The BIV model is able to well reproduce the main features of the claystone mechanical behavior in this loading path, such as the volume compressibility-dilatancy and confining stress sensitivity. The impact of mineralogical compositions is also correctly taken into account. Further, in Figure 15(a), the numerical results respectively provided by the associated and non-associated plastic model are compared. It is clear that the non-associated model gives a better prediction than the associated one.

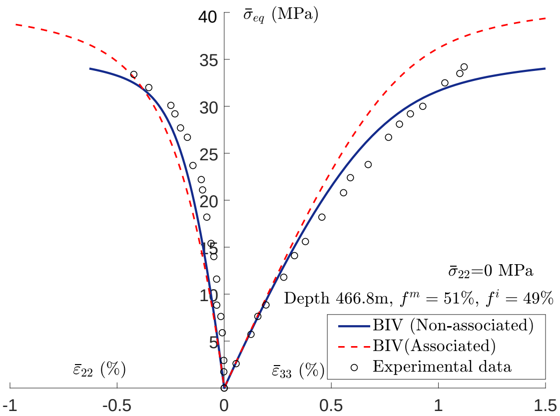

(a) Depth 466.8m, f^m = 51%, f^i = 49%,$\bar{\sigma}_{22}$ = 0 MPa

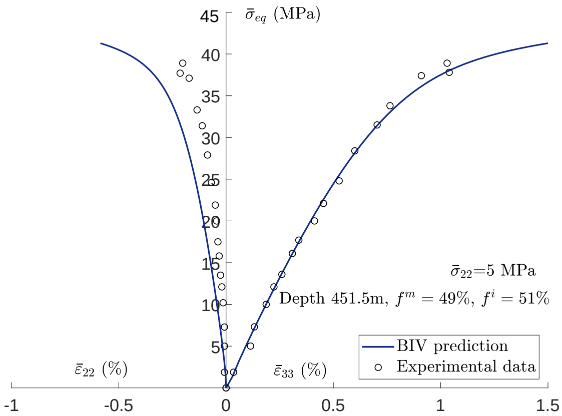

(b) Depth 451.5m, f^m = 49%, f^i = 51%,$\bar{\sigma}_{22}$ = 5 MPa

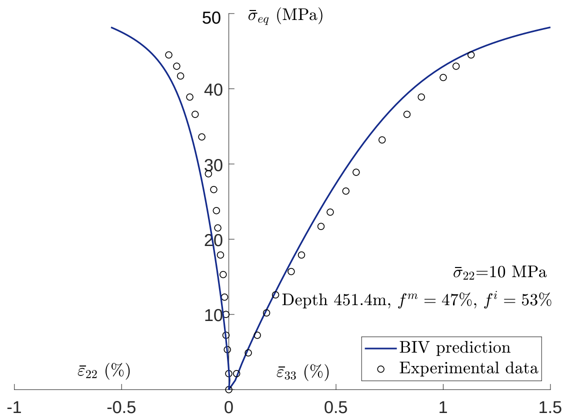

(c) Depth 451.4m, f^m = 47%, f^i = 53%,$\bar{\sigma}_{22}$ = 10 MPa

Figure 15: Comparison of stress-strain curves between experimental data and numerical results in triaxial compression tests on Callovo-Oxfordian claystone samples with different mineralogical compositions

For providing a complementary validation of the BIV model, proportional compression and lateral extension tests are also studied. In a proportional compression test, the axial stress $\bar{\sigma}_{33}$ and confining stress $\bar{\sigma}_{11}$ are simultaneously increased with a constant ratio $k = \frac{\bar{\sigma}_{33}}{\bar{\sigma}_{11}}$. In a lateral extension test, the sample is first subjected to a hydrostatic stress state to a desired value, and then the lateral stress $\bar{\sigma}_{11}$ is progressively decreased while the axial stress $\bar{\sigma}_{33}$ is kept constant. The comparisons between numerical predictions and experimental data for these two kinds of tests are shown in Figure 16 and 17, respectively. Again, one gets a good general agreement and the BIV model correctly reproduces the main characteristics of mechanical responses of the claystone in these two loading paths.

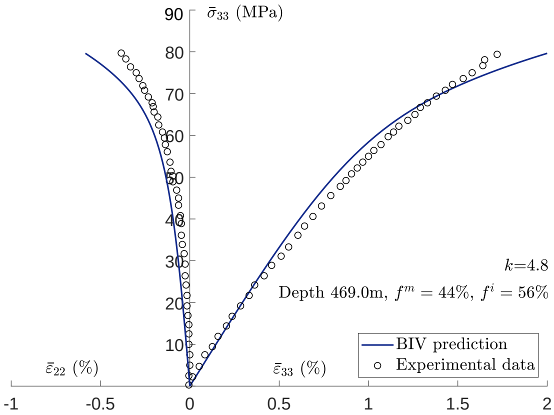

(a) Depth 469.0m, $f^m = 44\%$, $f^i = 56\%$, $k = 4.8$

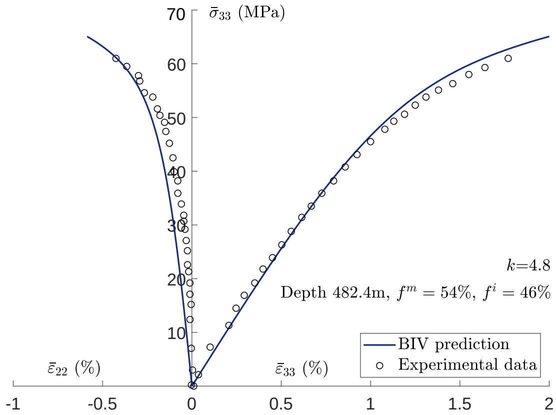

(b) Depth 482.4m, $f^m = 54\%$, $f^i = 46\%$, $k = 4.8$

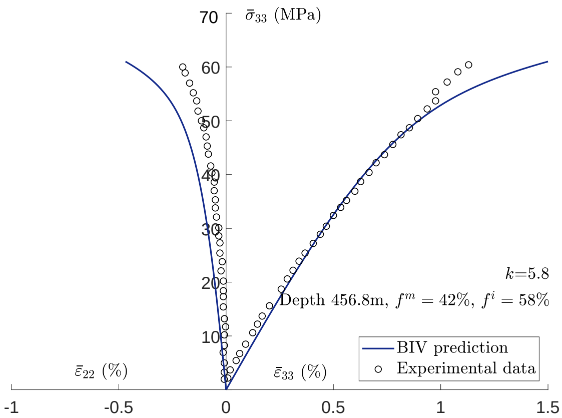

(c) Depth 456.8m, $f^m = 42\%$, $f^i = 58\%$, $k = 5.8$

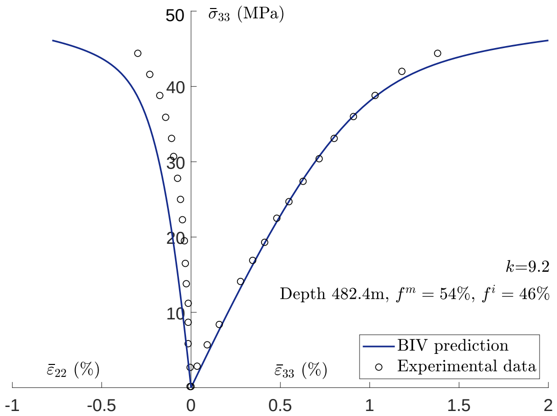

(d) Depth 482.4m, $f^m = 54\%$, $f^i = 46\%$, $k = 9.2$

Figure 16: Comparisons of mechanical responses between experimental data and numerical results in proportional compression tests on Callovo-Oxfordian claystone with different mineralogical compositions

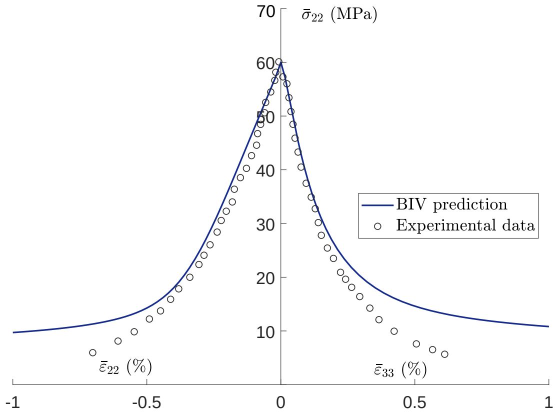

(a) Depth 469.0m, $f^m = 44\%$, $f^i = 56\%$

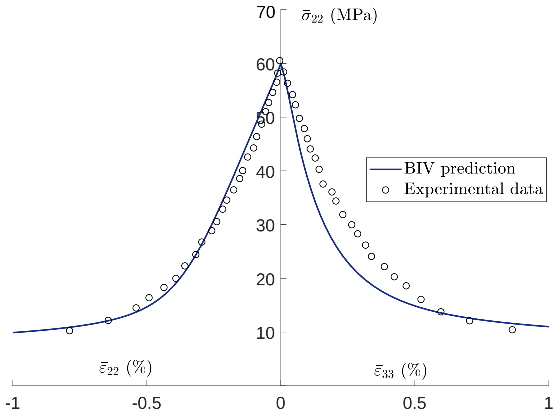

(b) Depth 482.3m, $f^m = 45\%$, $f^i = 55\%$

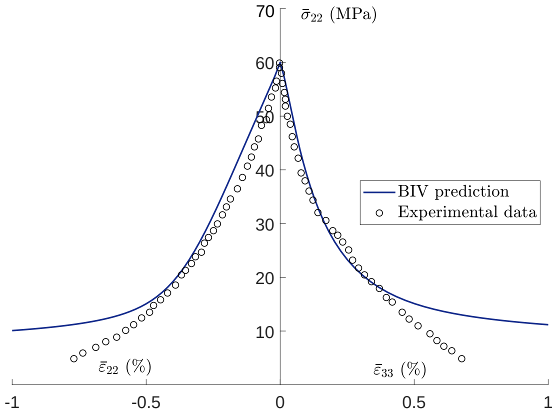

(c) Depth 456.6m, $f^m = 46\%$, $f^i = 54\%$

Figure 17: Comparisons of mechanical responses between experimental data and numerical results in lateral extension tests with an initial confining stress of 60MPa on Callovo-Oxfordian claystone with different mineralogical compositions

7.2.2. Application to Vosges sandstone

The Vosges sandstone is here studied as a typical porous rock. Its microstructure and macroscopic behaviors have been investigated in a number of previous studies, for instance (Khazraei, 1996, Bésuelle et al., 2000). The average porosity is about 20% and the solid matrix is composed of nearly 93% quartz grains with a few percent of feldspar and white mica. As a first approximation, the sandstone can be considered as an isotropic material. The mechanical strength of the sandstone strongly depends on confining pressure. In this study, the solid matrix is described by a non-associated plastic model based on the Drucker-Prager criterion. The elastic and plastic parameters of solid matrix are not directly measured but also indirectly estimated. The elastic coefficients can be easily identified by an inverse homogenization procedure from measured macroscopic values and the known porosity of sample. The plastic parameters are again fitted from a numerical optimization procedure of macroscopic stress-strain curves for a given porosity. The obtained values of parameters are given in Table

3.

Table 3: Parameters of solid matrix for porous Vosges sandstone

E^m (GPa)	ν^m	κ_0	κ_m	c(MPa)	b_1	χ_m	b_2
40	0.25	10^{-5}	0.433	40	900	0.333	500

In Figure 18, we first present the stress-strain curves in conventional triaxial compression tests with four different confining stresses from 5MPa to 40MPa. Like the claystone, there is a good agreement between model's predictions and experimental data. The effect of confining stress on macroscopic response is well captured. However, the mechanical strength of sandstone is slightly overestimated by the model for the test with a low confining stress of 5MPa. This is due to the fact that the linear Drucker-Prager criterion used for the solid matrix is not well adopted in the zone of low mean stress and tensile stress. The use of a curved yield surface for the solid matrix, for example the Mises-Schleicher criterion, would improve numerical results. In Figure 18(b), one can see that the non-associated model provides a better prediction of lateral strain that the associated model. However, unlike the result of claystone shown in Figure 15(a), the non-associated flow rule coefficient has no influence on the peak strength of porous sandstone.

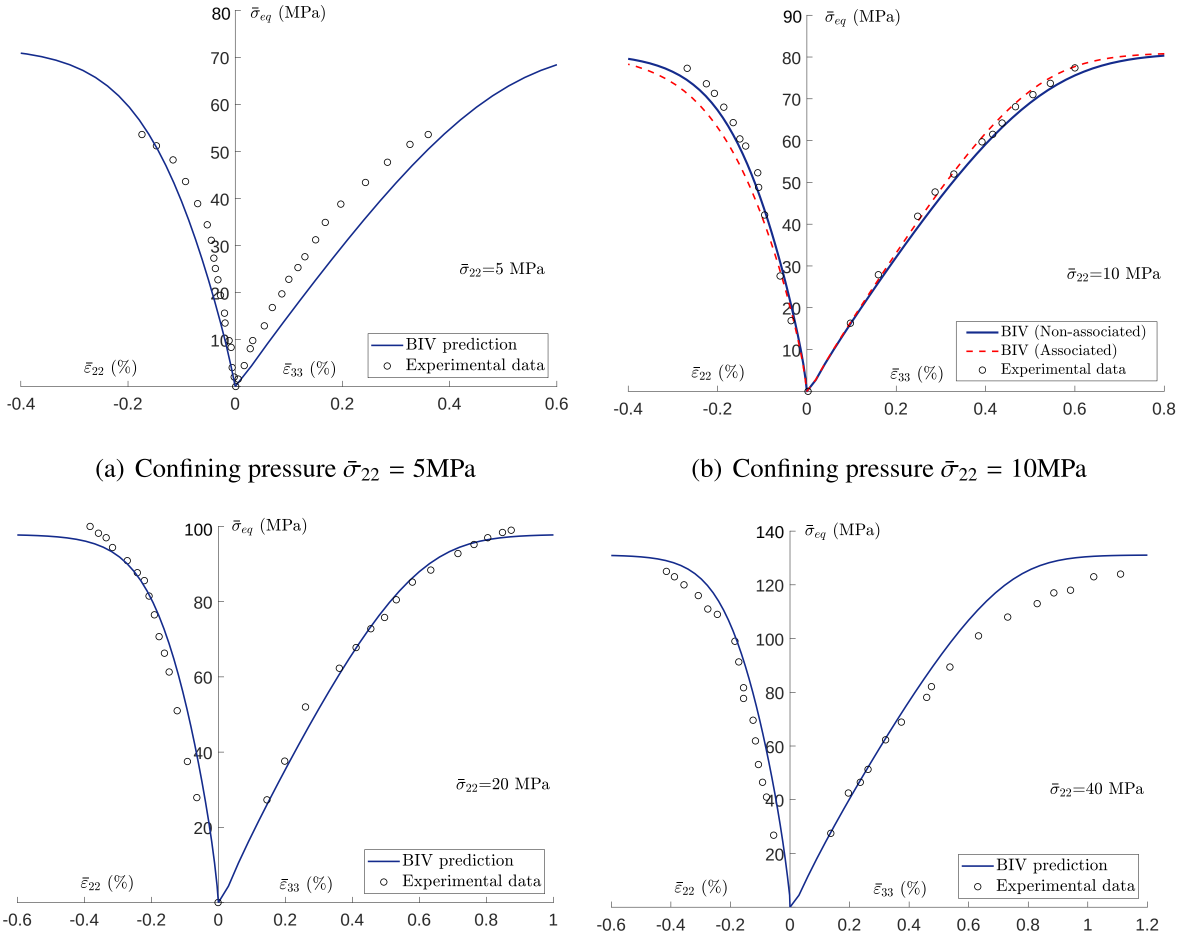

(a) Confining pressure $\bar{\sigma}_{22} = 5$MPa

(b) Confining pressure $\bar{\sigma}_{22} = 10$MPa

(c) Confining pressure $\bar{\sigma}_{22} = 20$MPa

(d) Confining pressure $\bar{\sigma}_{22} = 40$MPa

Figure 18: Comparisons of mechanical responses between experimental data and numerical results in triaxial compression tests on Vosges sandstone

The mechanical responses of Vosges sandstone in proportional compression and lateral extension tests are presented in Figures 19 and 20 respectively. Once more, it is found that the proposed BIV model well reproduce experimental data for these loading paths. In particular, as shown in Figure 19, the transition from volumetric compressibility to dilatancy is well reproduced by the BIV model due to the non-associated plastic flow rule used for the solid matrix.

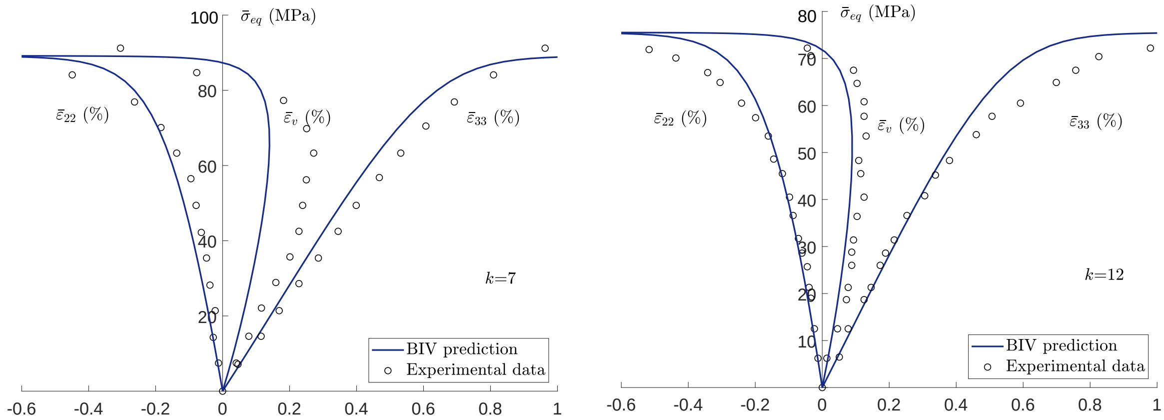

(a) $k = 7$ (b) $k = 12$

Figure 19: Comparison of stress-strain curves between experimental data and numerical results for proportional compression tests on Vosges sandstone

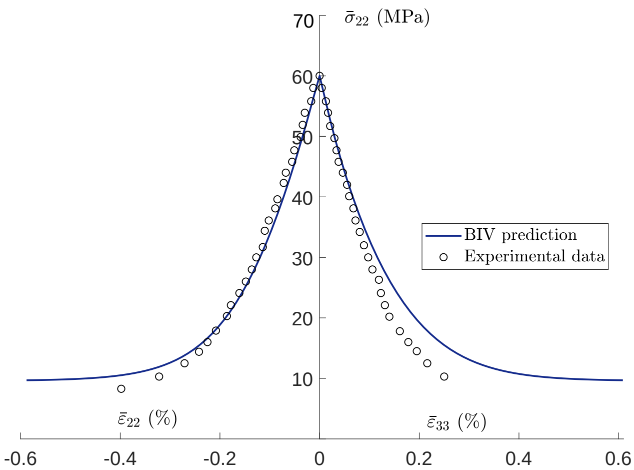

Figure 20: Comparison of mechanical response between experimental data and numerical results for lateral extension test on Vosges sandstone with an initial confining pressure of 60MPa and axial stress of 90MPa

8. Concluding remarks

In this paper, we have developed a new incremental variational framework for the estimation of effective elastic-plastic properties of a class of heterogeneous rocks by using the bi-potential theory. These materials are considered as implicit standard materials (ISMs). In particular, a bi-potential based incremental variational model (BIV) has been formulated for those rocks with a non-associated plastic matrix described by a Drucker-Prager type yield function and an isotropic hardening law.

The BIV model has first been formulated by considering an elastic perfectly plastic matrix phase. With the help of the bi-potential theory, we have determined the local incremental elastic and plastic bi-potentials of the matrix. We have also introduced an appropriate optimization method for the estimation of the effective incremental bi-potential and macroscopic stress. The accuracy of BIV model has been demonstrated through the comparisons with direct finite element simulations for both inclusion-reinforced composites and porous materials.

A heuristic extension of the BIV model has then been proposed in view of estimating effective behaviors of heterogeneous rocks exhibiting an isotropic plastic hardening. This has been done by assuming that the general incremental variational formulation obtained the perfectly plastic matrix remains applicable at each loading increment if the plastic hardening variables and functions are frozen. The plastic hardening has been taken into account by updating the values of the frozen hardening functions at each loading increment. The efficiency of the heuristically extended BIV model has also been confirmed by the comparisons with direct finite element simulations for both inclusion-reinforced composites and porous materials. It has been found that the BIV model was able to provide a good estimation of the fluctuations of local stress and plastic strain fields. However, the average stress in the inclusion phase was underestimated for the inclusion-reinforced composites while the stress fluctuation in the matrix phase is overestimated for both materials. Therefore, some improvement remains needed, for example, by using a second-order comparison composite for the estimation of incremental bi-potential of the plastic matrix.

Finally, the BIV model has been applied to studying the mechanical behavior of two typical geological materials, the Callovo-Oxifordian claystone and Vosges sandstone, under different loading paths. In a general way, the numerical results are in good agreement with experimental data. The main features of mechanical behaviors of two materials are correctly reproduced by the BIV model, such as influence of confining stress and volume compressibility-dilatancy transition.

In this work, we have focused on the short-term mechanical behavior of dry materials. In future, the BIV model is expected to be extended to the time-dependent behavior and to saturated and unsaturated materials. Moreover, it is acknowledged that the interfaces between the inclusions and the matrix play a non-negligible role in rocks plastic deformation and damage. The effects of interface will be also taken into account in our future work.

Acknowledgment

This study was jointly supported by the National Key RD Program of China (Grant No. 2017YFC1501100), the National Natural Science Foundation of China (Grant No.42001053), Key-Area Research and Development Program of Guang dong Province (Grant No. 2019B110205003) and China Postdoctoral Science Foundation funded project(Grant Nos. 2020M682638, 2020M682707).

Appendix A. Approximation of the local elastic bi-potential (24)

Inspired by Boudet et al. (2016), we assume that the volumetric plastic strain field $\boldsymbol{\beta}$ and the internal variable field γ^p are constant values in the solid matrix, denoted by $\langle\boldsymbol{\beta}\rangle_m$ and $\langle\gamma^p\rangle_m$, respectively. For the local stress state situated on the regular part of Drucker-Prager yield surface, the evolution of $\langle\boldsymbol{\beta}\rangle_m$ and $\langle\gamma^p\rangle_m$ can be expressed as follows by taking into account Eq. (31):

$$\langle\boldsymbol{\beta}\rangle_m = \langle\boldsymbol{\beta}_n\rangle_m + \overline{\overline{\dot{\boldsymbol{\alpha}}}}\Delta t \chi \boldsymbol{\delta} \tag{A.1}$$

$$\langle\gamma^p\rangle_m = \langle\gamma^p_n\rangle_m + \overline{\overline{\dot{\boldsymbol{\alpha}}}}\Delta t \tag{A.2}$$

where $\langle\boldsymbol{\beta}_n\rangle_m$ and $\langle\gamma^p_n\rangle_m$ are the volume average values of fields $\boldsymbol{\beta}$ and γ over the matrix phase at the step n, and

$$\overline{\overline{\dot{\boldsymbol{\alpha}}}} = \frac{1}{\Delta t}\sqrt{\frac{2}{3}\langle(\boldsymbol{\alpha}-\boldsymbol{\alpha}_n):(\boldsymbol{\alpha}-\boldsymbol{\alpha}_n)\rangle_m} = \frac{1}{\Delta t}\overline{\overline{\boldsymbol{\alpha}-\boldsymbol{\alpha}_n}} \tag{A.3}$$

Accordingly, one gets:

$$b^m_e(\boldsymbol{\varepsilon},\boldsymbol{\varepsilon}^p,\ \boldsymbol{\sigma}) \simeq b^{app}_e(\boldsymbol{\varepsilon},\boldsymbol{\alpha}) = \frac{1}{2}\boldsymbol{\sigma}:\mathbb{S}^m:\boldsymbol{\sigma}+\frac{1}{2}\left(\boldsymbol{\varepsilon}-\boldsymbol{\alpha}-\langle\boldsymbol{\beta}_n\rangle_m-\overline{\overline{\boldsymbol{\alpha}-\boldsymbol{\alpha}_n}}\chi\boldsymbol{\delta}\right):\mathbb{C}^m:\left(\boldsymbol{\varepsilon}-\boldsymbol{\alpha}-\langle\boldsymbol{\beta}_n\rangle_m-\overline{\overline{\boldsymbol{\alpha}-\boldsymbol{\alpha}_n}}\chi\boldsymbol{\delta}\right) \tag{A.4}$$

Appendix B. Minimization of $J^m_0(\boldsymbol{\varepsilon},\boldsymbol{\alpha})$

By making use of the minimization of $J^m_0(\boldsymbol{\varepsilon},\boldsymbol{\alpha})$ w.r.t. $\boldsymbol{\alpha}$, and after taking into account the relation (44) of J^m_0, one gets,

$$\frac{\partial J^m_0}{\partial\boldsymbol{\alpha}} = -\mathbb{K}:\ \mathbb{C}^m:(\boldsymbol{\varepsilon}-\boldsymbol{\alpha}-\langle\boldsymbol{\beta}\rangle_m)-\mathbb{C}^m:(\boldsymbol{\varepsilon}-\boldsymbol{\alpha}-\langle\boldsymbol{\beta}\rangle_m)\frac{\partial\langle\boldsymbol{\beta}\rangle_m}{\partial\boldsymbol{\alpha}}+2\frac{\eta_p\theta}{\Delta t}(\boldsymbol{\alpha}-\tilde{\boldsymbol{\alpha}}_n)=0 \tag{B.1}$$

It is noticed that Eq. (53) in its field form can be rewritten as:

$$\theta(\boldsymbol{\alpha}-\tilde{\boldsymbol{\alpha}}_n) = (\boldsymbol{\alpha}-\boldsymbol{\alpha}_n) \quad \forall \underline{x}\in\Omega_m \tag{B.2}$$

Considering the expression (A.1) and (B.2), one obtains

$$\frac{\partial\langle\boldsymbol{\beta}\rangle_m}{\partial\boldsymbol{\alpha}} = \frac{2\chi\theta}{3\Delta t\overline{\overline{\dot{\boldsymbol{\alpha}}}}}\boldsymbol{\delta}\otimes(\ \boldsymbol{\alpha}-\tilde{\boldsymbol{\alpha}}_n) \tag{B.3}$$

then

$$-\mathbb{C}^m:(\boldsymbol{\varepsilon}-\boldsymbol{\alpha}-\langle\boldsymbol{\beta}\rangle_m):\frac{\partial\langle\boldsymbol{\beta}\rangle_m}{\partial\ \boldsymbol{\alpha}} = 2\frac{\eta_{cp}\theta}{\Delta t}(\boldsymbol{\alpha}-\tilde{\boldsymbol{\alpha}}_n) \tag{B.4}$$

with

$$\eta_{cp} = \frac{-3\chi\sigma_m}{3\overline{\overline{\dot{\boldsymbol{\alpha}}}}},\quad \sigma_m = \frac{1}{3}\mathbb{C}^m:(\boldsymbol{\varepsilon}-\boldsymbol{\alpha}-\langle\ \boldsymbol{\beta}\rangle_m):\boldsymbol{\delta} \tag{B.5}$$

For ease of calculation, we assume that η_{cp} takes its average value in the matrix phase, i.e.:

$$\eta_{cp} = \frac{-3\chi \langle \sigma_m \rangle_m}{3\overline{\overline{\dot{\boldsymbol{\alpha}}}}} \tag{B.6}$$

Substituting Eqs. (B.2) and (B.4) into (B.1), ont gets:

$$\frac{\partial J_0^m}{\partial \boldsymbol{\alpha}} = -\mathbb{K} : \mathbb{C}^m : (\boldsymbol{\varepsilon} - \boldsymbol{\alpha} - \langle \boldsymbol{\beta} \rangle_m) + 2\frac{\eta\theta}{\Delta t}(\boldsymbol{\alpha} - \tilde{\boldsymbol{\alpha}}_n) = 0 \tag{B.7}$$

with

$$\eta = \eta_p + \eta_{ih} + \eta_{cp} = \frac{\left\langle \sigma_y \right\rangle_m - 3\chi \langle \sigma_m \rangle_m}{3\overline{\overline{\dot{\boldsymbol{\alpha}}}}} = -\frac{\kappa\left(\langle \sigma_m \rangle_m - c\right)}{\overline{\overline{\dot{\boldsymbol{\alpha}}}}} \tag{B.8}$$

or equivalently, the local deviatoric stress of matrix phase becomes:

$$\boldsymbol{s} = \mathbb{K} : \mathbb{C}^m : (\boldsymbol{\varepsilon} - \boldsymbol{\alpha} - \langle \boldsymbol{\beta} \rangle_m) = 2\frac{\eta}{\Delta t}(\boldsymbol{\alpha} - \boldsymbol{\alpha}_n) = 2\frac{\eta\theta}{\Delta t}(\boldsymbol{\alpha} - \tilde{\boldsymbol{\alpha}}_n) \tag{B.9}$$

Finally, from (B.7), one gets

$$\boldsymbol{\alpha} = \left(\mathbb{C}^m + \frac{2\theta\eta}{\Delta t}\mathbb{K}\right)^{-1} : \left[\mathbb{K} : \mathbb{C}^m : \boldsymbol{\varepsilon} + \frac{2\theta\eta}{\Delta t}\tilde{\boldsymbol{\alpha}}_n\right] \tag{B.10}$$

Appendix C. Effective behavior and field statistics of RVE

The effective potential $\Pi_0(\bar{\boldsymbol{\varepsilon}})$ is written as

$$\Pi_0(\bar{\boldsymbol{\varepsilon}}) = \frac{1}{2}\bar{\boldsymbol{\varepsilon}} : \bar{\mathbb{C}} : \bar{\boldsymbol{\varepsilon}} + \bar{\boldsymbol{\rho}} : \bar{\boldsymbol{\varepsilon}} + \bar{\zeta} \tag{C.1}$$

where

$$\bar{\mathbb{C}} = f^m \mathbb{C}_0^m : \mathbb{A}^m + \sum_{r=1}^{N} f^{i,r}\mathbb{C}^{i,r} : \mathbb{A}^{i,r} \tag{C.2a}$$

$$\bar{\boldsymbol{\rho}} = f^m \boldsymbol{\rho}_0^m : \mathbb{A}^m \tag{C.2b}$$

$$\bar{\zeta} = f^m\left(\zeta_0^m + \boldsymbol{\rho}_0^m : \boldsymbol{a}^m\right) \tag{C.2c}$$

The average of the local strain filed in the matrix can be related to the macroscopic strain by two strain concentration tensors $\mathbb{A}^m$, $\boldsymbol{a}^m$, i.e., (Willis, 1981)

$$\langle \boldsymbol{\varepsilon} \rangle_m = \mathbb{A}^m : \bar{\boldsymbol{\varepsilon}} + \boldsymbol{a}^m \tag{C.3}$$

and similarly, the average of local strain filed in the r^{th} inclusion phase can also be described by:

$$\langle \boldsymbol{\varepsilon} \rangle_{i,r} = \mathbb{A}^{i,r} : \bar{\boldsymbol{\varepsilon}} + \boldsymbol{a}^{i,r} \tag{C.4}$$

Note that the fourth-order tensors $\mathbb{A}^m$ and $\mathbb{A}^{i,r}$ can be identified to those computed for the composites in the purely elastic case. However, the expressions of second-order tensors $\boldsymbol{a}^m$ and $\boldsymbol{a}^{i,r}$ should be calculated by the volume averaging in each phase.

The second-order moment of strain filed $\boldsymbol{\varepsilon}$ in the matrix phase can be obtained from the effective free energy $\Pi_0\left(\bar{\boldsymbol{\varepsilon}}\right)$ and by using the relations (Castañeda, 2002, Lahellec and Suquet, 2007b):

$$\langle \boldsymbol{\varepsilon} \otimes \boldsymbol{\varepsilon} \rangle_m = \frac{2}{f^m} \frac{\partial \Pi_0}{\partial \mathbb{C}_0^m} \tag{C.5}$$

Note that $\mathbb{C}_0^m$ can be expressed by two effective moduli as $\mathbb{C}_0^m = 3k^m\ \mathbb{J} + 2\mu_0^m\ \mathbb{K}$. Then the deviatoric part of this second order moment gives (Huang et al., 2015, Lahellec and Suquet, 2007a)

$$\mathbb{K} :: \langle \boldsymbol{\varepsilon} \otimes \boldsymbol{\varepsilon} \rangle_m = \frac{1}{f^m} \frac{\partial \Pi_0}{\partial \mu_0^m} \tag{C.6}$$

In order to take advantage of the explicit expression of the tensors $\mathbb{A}^m$, $\mathbb{A}^{i,r}$, $\boldsymbol{a}^m$ and $\boldsymbol{a}^{i,r}$, a two-phase material, one phase of elastic inclusion ($r = N = 1$) and another phase of elastic-plastic matrix, is considered for validation and application. In this case, the fourth order concentration tensors associated to the Hashin-Shtrikman (HS) estimates are adopted (Hashin, 1962)

$$\mathbb{A}^m = \mathbb{I} + \frac{1}{f^m}\left(\mathbb{C}_0^m - \mathbb{C}^{i,r}\right)^{-T} : \left(\bar{\mathbb{C}} - \langle \mathbb{C} \rangle\right)^T \tag{C.7a}$$

$$\mathbb{A}^{i,r} = \mathbb{I} + \frac{1}{f^{i,r}}\left(\mathbb{C}^{i,r} - \mathbb{C}_0^m\right)^{-T} : \left(\bar{\mathbb{C}} - \langle \mathbb{C} \rangle\right)^T \tag{C.7b}$$

$$\boldsymbol{a}^m = \left(\mathbb{C}_0^m - \mathbb{C}^{i,r}\right)^{-1} : \left(\mathbb{I} - \mathbb{A}_m\right)^T : \boldsymbol{\rho}_0^m \tag{C.7c}$$

$$\boldsymbol{a}^{i,r} = -\left(\mathbb{C}^{i,r} - \mathbb{C}_0^m\right)^{-1} : \left(\mathbb{I} - \mathbb{A}_{i,r}\right)^T : \boldsymbol{\rho}_0^m \tag{C.7d}$$

where $\langle \mathbb{C} \rangle = f^m \mathbb{C}_0^m + f^{i,r}\ \mathbb{C}^{i,r}$.

References

Agoras, M., Avazmohammadi, R., Castañeda, P. P., 2016. Incremental variational procedure for elasto-viscoplastic composites and application to polymer-and metal-matrix composites reinforced by spheroidal elastic particles. International Journal of Solids and Structures 97, 668–686.

Armand, G., Conil, N., Talandier, J., Seyedi, D. M., 2016. Fundamental aspects of the hydromechanical behaviour of callovo-oxfordian claystone: From experimental studies to model calibration and validation. Computers & Geotechnics.

Berga, A., 2012. Mathematical and numerical modeling of the non-associated plasticity of soils—part 1: The boundary value problem. International Journal of Non-Linear Mechanics 47 (1), 26–35.

Bésuelle, P., Desrues, J., Raynaud, S., 2000. Experimental characterisation of the localisation phenomenon inside a vosges sandstone in a triaxial cell. International Journal of Rock Mechanics and Mining Sciences 37 (8), 1223–1237.

Bodovillé, G., 2001. On generalised and implicit normality hypotheses. Meccanica 36 (3), 273–290.

Bodovillé, G., De Saxcé, G., 2001. Plasticity with non-linear kinematic hardening: modelling and shakedown analysis by the bipotential approach. European Journal of Mechanics-A/Solids 20 (1), 99–112.

Boudet, J., Auslender, F., Bornert, M., Lapusta, Y., 2016. An incremental variational formulation for the prediction of the effective work-hardening behavior and field statistics of elasto-(visco)plastic composites. International Journal of Solids & Structures 83, 90–113.

Brassart, L., Stainier, L., Doghri, I., Delannay, L., 2011. A variational formulation for the incremental homogenization of elasto-plastic composites. Journal of the Mechanics and Physics of Solids 59 (12), 2455–2475.

Brassart, L., Stainier, L., Doghri, I., Delannay, L., 2012. Homogenization of elasto-(visco) plastic composites based on an incremental variational principle. International Journal of Plasticity 36, 86–112.

Castañeda, P. P., 2002. Second-order homogenization estimates for nonlinear composites incorporating field fluctuations: I-theory. Journal of the Mechanics & Physics of Solids 50 (4), 737–757.

Castañeda, P. P., 1991. The effective mechanical properties of nonlinear isotropic composites. Journal of the Mechanics and Physics of Solids 39 (1), 45–71.

Castañeda, P. P., 1992. New variational principles in plasticity and their application to composite materials. Journal of the Mechanics and Physics of Solids 40 (8), 1757–1788.

Castañeda, P. P., 2002. Second-order homogenization estimates for nonlinear composites incorporating field fluctuations: I theory. Journal of the Mechanics and Physics of Solids 50 (4), 737–757.

Castañeda, P. P., Suquet, P., 1997. Nonlinear composites. In: Advances in applied mechanics. Vol. 34. Elsevier, pp. 171–302.

Castañeda, P. P., Willis, J., 1999. Variational second-order estimates for nonlinear composites. In: Proceedings of the Royal Society of London A: Mathematical, Physical and Engineering Sciences. Vol. 455. The Royal Society, pp. 1799–1811.

Chaboche, J., Kanouté, P., Roos, A., 2005. On the capabilities of mean-field approaches for the description of plasticity in metal matrix composites. International journal of Plasticity 21 (7), 1409–1434.

Chiarelli, A.-S., 2000. Etude expérimentale et modélisation du comportement mécanique de l'argilité de l'est: influence de la profondeur et de la teneur en eau.

Danas, K., Castañeda, P. P., 2012. Influence of the lode parameter and the stress triaxiality on the failure of elasto-plastic porous materials. International Journal of Solids and Structures 49 (11-12), 1325–1342.

De Saxcé, G., 1995. The bipotential method, a new variational and numerical treatment of the dissipative laws of materials. In: Proc. 10th Int. Conf. on Mathematical and Computer Modelling and Scientific Computing,(Boston, 1995).

De Saxcé, G., Bousshine, L., 1998. Limit analysis theorems for implicit standard materials: Application to the unilateral contact with dry friction and the non-associated flow rules in soils and rocks. International Journal of Mechanical Sciences 40 (4), 387–398.

De Saxcé, G., Feng, Z.-Q., 1991. New inequality and functional for contact with friction: The implicit standard material approach. Journal of Structural Mechanics 19 (3), 301–325.

Fenchel, W., 1949. On conjugate convex functions. Canadian Journal of Mathematics 1 (1), 73–77.

Guéry, A. C., Cormery, F., Shao, J. F., Kondo, D., 2008. A micromechanical model of elastoplastic and damage behavior of a cohesive geomaterial. International Journal of Solids & Structures 45 (5), 1406–1429.

Guéry, A. C., Cormery, F., Shao, J. F., Kondo, D., 2010. A multiscale modeling of damage and time-dependent behavior of cohesive rocks. International Journal for Numerical & Analytical Methods in Geomechanics 33 (5), 567–589.

Halphen, B., Nguyen, Q. S., 1975. Sur les matériaux standard généeralisés.

Hashin, Z., 1962. The elastic moduli of heterogeneous materials. Journal of Applied Mechanics 29 (1), 2938–2945.

Hill, R., 1965. Continuum micro-mechanics of elastoplastic polycrystals. Journal of the Mechanics and Physics of Solids 13 (2), 89–101.

Hjiaj, M., Fortin, J., De Saxcé, G., 2003. A complete stress update algorithm for the non-associated drucker–prager model including treatment of the apex. International Journal of Engineering Science 41 (10), 1109–1143.

Huang, Y., Guéry, A. C., Shao, J. F., 2015. Incremental variational approach for time dependent deformation in clayey rock. International Journal of Plasticity 64, 88–103.

Idiart, M. I., Castañeda, P. P., 2007. Field statistics in nonlinear composites. i. theory 463 (2077), 183–202.

Jiang, T., Guéry, A. A.-C., Kondo, D., Shao, J.-F., 2009. Multi-scale modeling for inelastic behavior of a cohesive geomaterial. Mechanics Research Communications 36 (6), 673–681.

Jiang, T., Shao, J.-F., 2009. On the incremental approach for nonlinear homogenization of composite and influence of isotropization. Computational Materials Science 46 (2), 447–451.

Khazraei, R., 1996. Experimental study and modeling of damage in brittle rocks. Ph.D. thesis, University of Lille, Lille,France.

Lahellec, N., Suquet, P., 2007a. Effective behavior of linear viscoelastic composites: a time-integration approach. International Journal of Solids and Structures 44 (2), 507–529.

Lahellec, N., Suquet, P., 2007b. On the effective behavior of nonlinear inelastic composites: I. incremental variational principles. Journal of the Mechanics and Physics of Solids 55 (9), 1932–1963.

Lahellec, N., Suquet, P., 2013. Effective response and field statistics in elasto-plastic and elasto-viscoplastic composites under radial and non-radial loadings. International Journal of Plasticity 42, 1–30.

Lide, D. R., 2004. Handbook of Chemistry and Physics. CRC Press.

Ortiz, M., Stainier, L., 1999. The variational formulation of viscoplastic constitutive updates. Computer Methods in Applied Mechanics & Engineering 171 (3), 419–444.

Robinet, J. C., 2008. Minéralogie, porosité et diffusion des solutés dans l'argilite du callovo-oxfordien de bure (meuse, haute-marne, france) de l'échelle centimétrique à micrométrique. Bibliogr.

Shen, W., Shao, J.-F., Kondo, D., Gatmiri, B., 2012. A micro–macro model for clayey rocks with a plastic compressible porous matrix. International journal of plasticity 36, 64–85.

Suquet, P., 1996. Overall properties of nonlinear composites. In: IUTAM Symposium on Micromechanics of Plasticity and Damage of Multiphase Materials. Springer, pp. 149–156.

Willis, J. R., 1981. Variational and related methods for the overall properties of composites. Advances in Applied Mechanics 21, 1–78.

Yan, Y., Geng, L., Li, A., 2007. Experimental and numerical studies of the effect of particle size on the deformation behavior of the metal matrix composites. Materials Science and Engineering: A 448 (1-2), 315–325.

Zhang, K., Zhao, L.-Y., Ni, T., Zhu, Q.-Z., Shen, J., Fan, Y.-H., 2019. Experimental investigation and multiscale modeling of reactive powder cement pastes subject to triaxial compressive stresses. Construction and Building Materials 224, 242–254.

Zhao, L.-Y., Shao, J.-F., Zhu, Q.-Z., Liu, Z.-B., Yurtdas, I., 2019. Homogenization of rock-like materials with plastic matrix based on an incremental variational principle. International Journal of Plasticity.
URL http://www.sciencedirect.com/science/article/pii/S074964191830634X

Zhao, L.-Y., Zhu, Q.-Z., Shao, J.-F., 2018. A micro-mechanics based plastic damage model for quasi-brittle materials under a large range of compressive stress. International Journal of Plasticity 100, 156–176.

Zhu, Q., Kondo, D., Shao, J., 2008. Micromechanical analysis of coupling between anisotropic damage and friction in quasi brittle materials: role of the homogenization scheme. International Journal of Solids and Structures 45 (5), 1385–1405.

Zhu, Q. Z., Zhao, L. Y., Shao, J. F., 2016. Analytical and numerical analysis of frictional damage in quasi brittle materials. Journal of the Mechanics and Physics of Solids 92, 137–163.

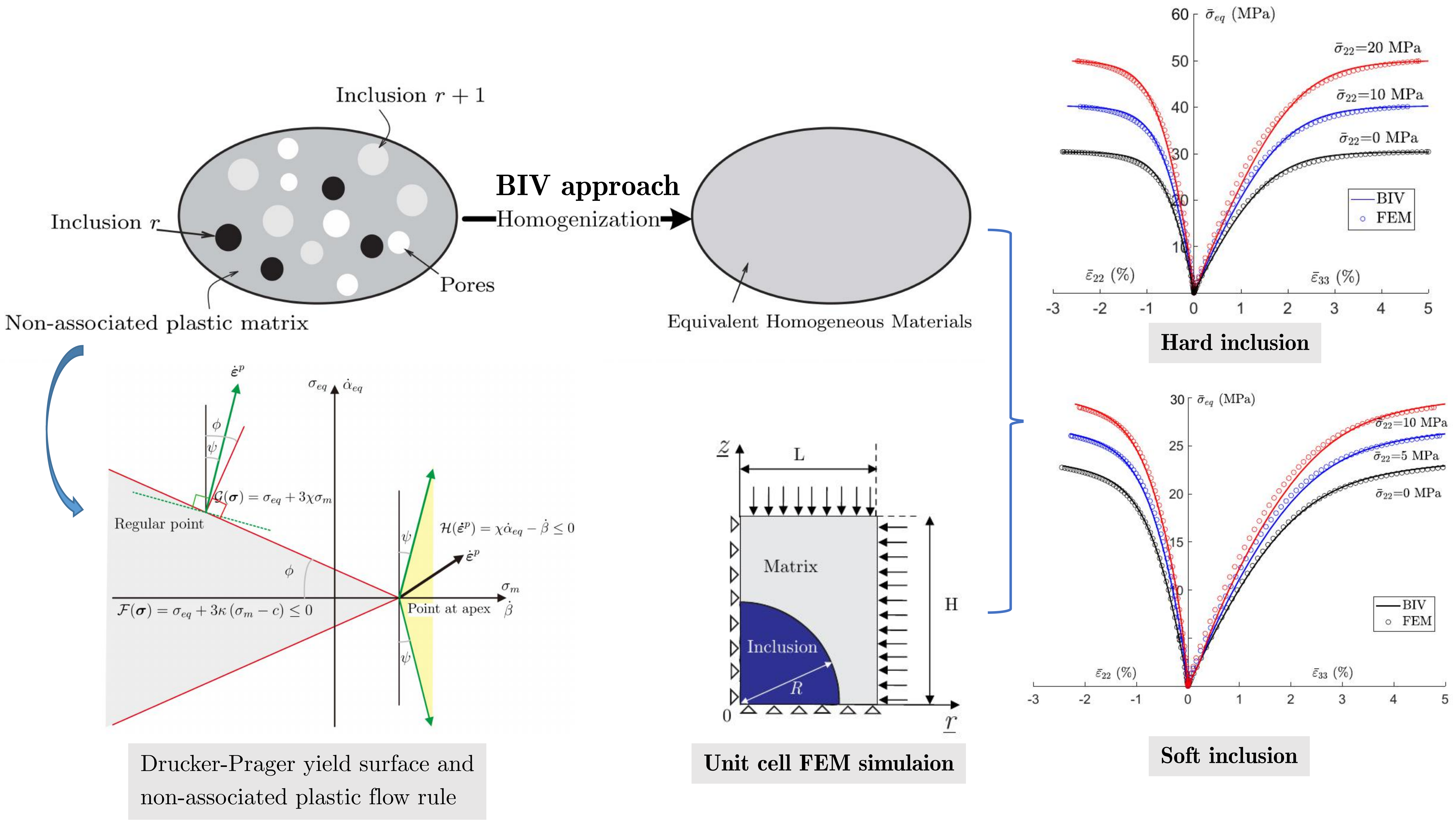
Inclusion $r+1$
Inclusion r
Pores
Non-associated plastic matrix
BIV approach
Homogenization
Equivalent Homogeneous Materials
$\dot{\varepsilon}^p$
σ_{eq} $\dot{\alpha}_{eq}$
ϕ
ψ
$\mathcal{G}(\boldsymbol{\sigma}) = \sigma_{eq} + 3\chi\sigma_m$
Regular point
$\mathcal{H}(\dot{\varepsilon}^p) = \chi\dot{\alpha}_{eq} - \dot{\beta} \leq 0$
σ_m
$\dot{\beta}$
$\mathcal{F}(\boldsymbol{\sigma}) = \sigma_{eq} + 3\kappa(\sigma_m - c) \leq 0$
Point at apex
Drucker-Prager yield surface and non-associated plastic flow rule
z
L
Matrix
H
Inclusion
R
0
r
Unit cell FEM simulaion
$\bar{\sigma}_{eq}$ (MPa)
$\bar{\sigma}_{22}$=20 MPa
$\bar{\sigma}_{22}$=10 MPa
$\bar{\sigma}_{22}$=0 MPa
BIV
FEM
$\bar{\varepsilon}_{22}$ (%)
$\bar{\varepsilon}_{33}$ (%)
Hard inclusion
$\bar{\sigma}_{eq}$ (MPa)
$\bar{\sigma}_{22}$=10 MPa
$\bar{\sigma}_{22}$=5 MPa
$\bar{\sigma}_{22}$=0 MPa
BIV
FEM
$\bar{\varepsilon}_{22}$ (%)
$\bar{\varepsilon}_{33}$ (%)
Soft inclusion